Figure 2. Histopathology of anaplastic lymphoma kinase (ALK)-positive renal cancer. Cuboidal tumor cells showed papillary, tubular, or cribriform growth patterns. The tumor cells had eosinophilic cytoplasm and round to ovoid nuclei. (A) The glandular structures possessed abundant mucin. (D) The tumor comprised a papillary structure of cuboidal or low columnar cells, with eosinophilic cytoplasm and small uniform round to oval nuclei (A,D hematoxylin and eosin stain). The tumor cells were (B) weakly positive and (E) indeterminate for ALK with conventional anti-ALK immunohistochemistry. (C,F) All of the tumor cells were clearly positive for ALK when the iAEP method was used. The staining pattern was diffuse cytoplasmic, with (C) membranous or (F) fine granular accentuation. Figures were taken using the corresponding whole sections (× 10 objective for low power view. × 40 objective for inset). Case 1 (A-C); Case 2 (D-F).

probes for ALK (RP11-984I21, RP11-62B19, RP11-701P18), TPM3 (RP11-809B24), and EML4 (RP11-996L7). Hybridized slides were then stained with 4',6-diamidino-2-phenylindole and examined using a fluorescence microscope BX51 (Olympus, Tokyo, Japan).

Mutation Analyses for MET

A 1007-bp cDNA fragment containing the MET kinase domain was amplified using the primers MET-3186F (5'-GTCCATTACTGCAAAATACTGTCC-3') and MET-4193R (5'-CACCTCATCATCAGCGTTATC-3'). The PCR product was sequenced after subcloning.

RESULTS

Identification of ALK Fusions in RCC Samples

Sections of tissue microarray were immunostained for ALK by the iAEP method, resulting in the detection of 2 positive cases (case 1, Fig. 2A-C; case 2, Fig. 2D-F). The positive results were also confirmed using corresponding whole histopathological sections, in which all of the tumor cells stained for ALK as other ALK-positive cancers usually do. We carried out 5'-RACE assays to determine whether these cases expressed ALK fusion or full-length ALK (mutated or unmutated). We isolated a cDNA fragment containing the exon 8 of *TPM3* fused in-frame to

the exon 20 of *ALK* (Fig. 3A) in case 1, and the exon 2 of *EML4* fused to the exon 20 of *ALK* in case 2 (Fig. 3B). This EML4-ALK is called variant 5 (E2;A20) in lung cancer.[30] Reverse transcription PCR (RT-PCR) assays designed for the *TPM3-ALK* or E2;A20 successfully amplified cDNAs containing the fusion points (Fig. 3C,D). To confirm the genomic rearrangement, we performed FISH assays (Fig. 4) and genomic PCR (data not shown) for each fusion. All our results were consistent with the presence of t(1;2)(p21;p23)/*TPM3-ALK* in case 1, or inv(2)(p21p23)/E2;A20 in case 2. No other cases were positive for ALK by iAEP immunohistochemistry. All 355 cases were further examined by ALK-split FISH assay. In 12 of the cases, FISH was unsuccessful and not evaluable. In the other cases, the results were identical to those obtained by anti-ALK iAEP immunohistochemistry.

Case Presentation

Case 1

The patient was a 36-year-old woman who had a complaint suggestive of pyelonephritis. Magnetic resonance imaging and computed tomography showed a mass (4.0 cm × 4.0 cm × 3.5 cm) in the left kidney. No metastatic lesions or lymph node enlargements were identified. The patient had no past medical history of malignancy.
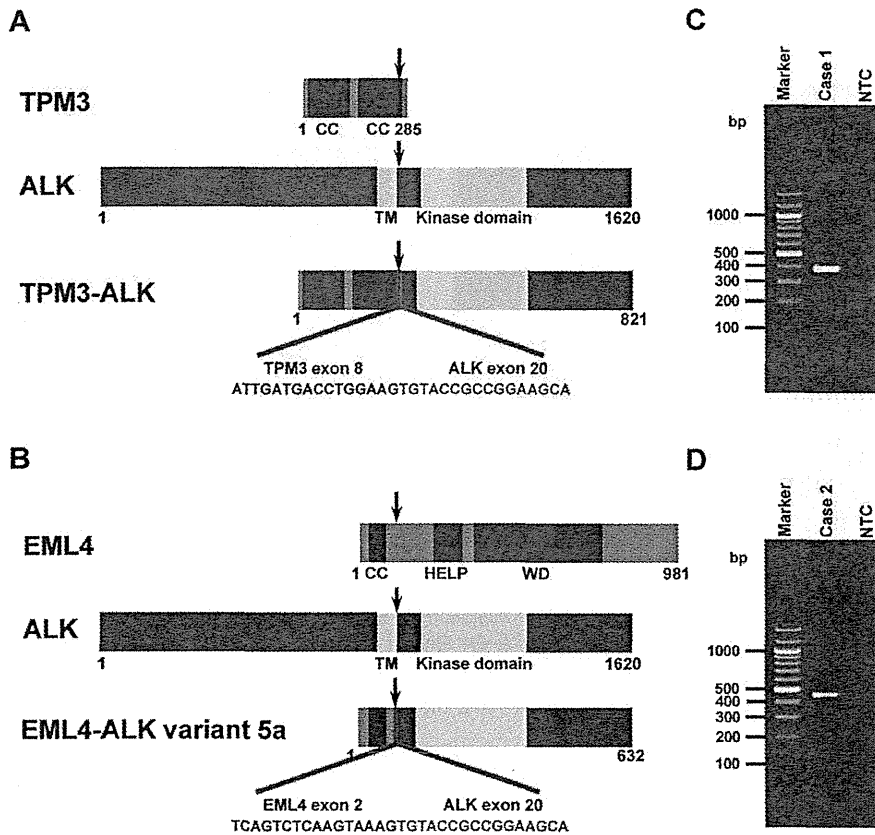
4

Figure 3. Identification of anaplastic lymphoma kinase (ALK) fusions. Tropomyosin 3 (TPM3) harbors 2 coiled-coil domains. (A) Case 1. A chromosome translocation generates a fusion protein in which the 2 coiled-coil domains of TPM3 and the intracellular region of ALK (containing the tyrosine kinase domain) are conserved. (B) Nucleotide sequencing of the polymerase chain reaction (PCR) products in case 2 revealed that exon 2 of echinoderm microtubule-associated protein like 4 (EML4), comprising a coiled-coil domain, was fused to exon 20 of ALK, generating the variant 5 complementary DNA (cDNA). In TPM3 and EML4 fusions, the region containing the coiled-coil domain is fused to the kinase domain of ALK. Numbers indicate amino acid positions of each protein. Arrow indicates the chromosomal breakpoint. The cDNA fragments of 385 base pairs (bp) and 454 bp were obtained by reverse transcription PCR, corresponding to (C) *TPM3-ALK* and (D) *EML4-ALK* variant 5, respectively. The left lane ("Marker") contains DNA size standards (100-bp ladder). CC indicates coiled-coil domain; HELP, hydrophobic echinoderm microtubule-associated protein; NTC, no-template control; TM, transmembrane domain; WD, WD repeats.

She underwent a translumbar left-radical nephrectomy and is currently alive and well without evidence of disease at 2 years of follow-up.

Case 2

A 53-year-old woman was found incidentally to have microscopic hematuria by medical check-up. Ultrasonography and magnetic resonance imaging showed a change in the left kidney, but the diagnosis was indefinite at that time. One year later, adenocarcinoma cells were detected by urinary cytology, and computed tomography revealed an isodence left renal mass (2.5 cm × 2.5 cm × 2.3 cm). The patient underwent a translumbar left-radical nephrectomy. She is currently alive and well at 7 years after surgery.

The patients had no episodes or family history indicative of sickle cell trait. To the best of our knowledge, there is no reported case of (genetically) Japanese individuals with sickle cell trait/disease.

Histopathological Examinations

The 2 ALK-positive renal cancers were papillary subtype and unclassified (with mixed features of papillary, mucinous cribriform, and solid patterns with rhabdoid cells). They comprised 2.3% of non–clear cell RCCs (2 of 88) and 3.7% of non–clear cell and nonchromophobe RCCs (2 of 54).

Case 1

Histologically, tumor cells were composed of papillary, tubular, or cribriform growth of cuboidal cells with
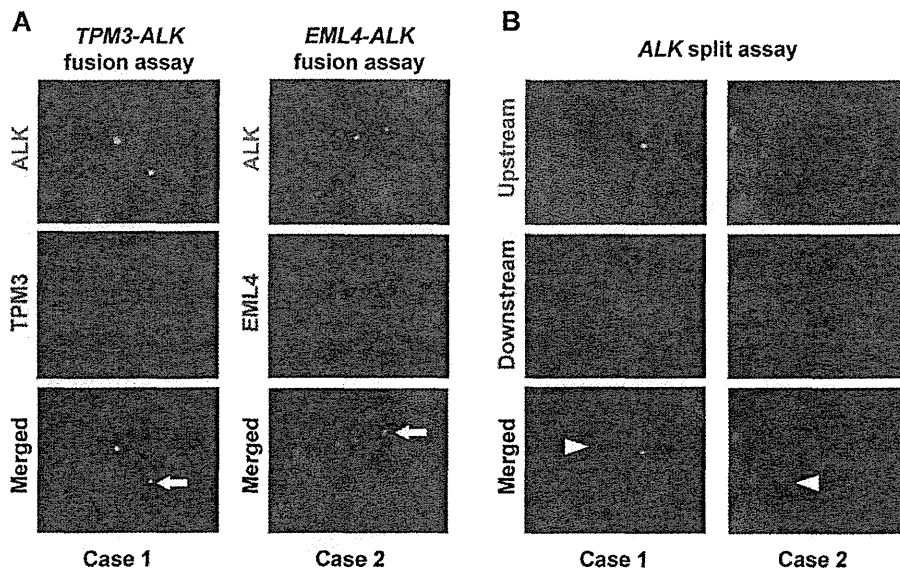
Figure 4. Fluorescence in situ hybridization analyses for *TPM3-ALK* (tropomyosin 3 fusion with anaplastic lymphoma kinase) and *EML4-ALK* (echinoderm microtubule-associated protein like 4 fusion with ALK). (A) In the *TPM3-ALK* and *EML4-ALK* fusion assays, the fusion genes are indicated by arrows. (B) The same clinical specimens as in (A) were subjected to fluorescence in situ hybridization analysis with differentially labeled probes for the upstream (green) or downstream (red) to the ALK breakpoint. In each case, the absence of 1 upstream signal indicated ALK rearrangement. Arrowhead indicates the rearranged ALK. The color of fluorescence for the bacterial artificial chromosome clones and the case numbers are indicated. Nuclei are stained blue with 4',6-diamidino-2-phenylindole.

eosinophilic cytoplasm. The cribriform morphology consisted of tubular structures with flattened epithelial cells, compressed by mucinous pool and inter- or intracytoplasmic vacuoles. Solid sheets of tumor cells with occasional deeply eosinophilic intracytoplasmic inclusions and eccentric nuclei, resulting in rhabdoid features, were focally identified. Nuclei were round to ovoid, and the nuclear size was basically uniform. Irregular nuclear membranes and nuclear grooves were occasionally observed. Mitotic figures were scant. The background stroma in the tumor area possessed abundant mucin. Frequent deposition of psammoma bodies and infiltration of numerous foamy macrophages were also seen. A large amount of mucinous matrix was highlighted with Alcian blue stain. These histological features resembled the mucinous cribriform pattern frequently observed in ALK-positive lung adenocarcinoma,[18,31] and also a representative case of unclassified RCC by Lopez-Beltran et al,[32] favoring a diagnosis of unclassified RCC. Immunohistochemically, neoplastic cells showed a diffuse and strong positivity for ALK (iAEP), vimentin, EMA, cytokeratin 7, AE1/AE3, cytokeratin CAM5.2, and cytokeratin 34βE12, and focally staining for PAX2, PAX8, AMACR, and CD10. TTF1 and RCC Ma were completely negative. Intracytoplasmic inclusions corresponded to aggregates of interme-

diate filaments of vimentin. The ALK-staining pattern appeared to be accentuated around the cell membrane of rhabdoid cells. The MIB1 (mindbomb homolog 1) labeling index was less than 1%.

Case 2

Histologically, the tumor consisted of papillary configuration of cuboidal or low columnar cells, with eosinophilic cytoplasm and small uniform round to oval nuclei. A clear cell change was focally seen. Nuclei showed a round to oval shape, and nuclear grooves were frequently observed. The size variation of nuclei was minimal, and the irregularity of the nuclear membrane was evident. Nuclear pseudoinclusions were seldom seen. Small nucleoli were occasionally identified, but mitoses were absent. The fibrovascular cores of papillary architecture contained numerous psammoma bodies and foamy macrophages. In addition, glandular lumens of tumor cells focally contained myxoid materials. These findings morphologically corresponded to papillary RCC, but did not fit to types 1 and 2 by the classification of Delahunt and Eble.[33] In contrast, the features resembled papillary RCC, type 2A, described by Yang et al.[34] Alcian blue stain highlighted a small amount of stromal-type mucin. Upon immunohistochemical analysis, neoplastic cells were diffusely and

strongly positive for ALK (iAEP), vimentin, EMA, cytokeratin 7, AE1/AE3, cytokeratin CAM5.2, cytokeratin 34βE12, and AMACR, and focally positive for PAX2 and PAX8, but negative for TTF1, CD10, and RCC Ma.

Examinations of Other Gene Aberrations

For *MET*, a cDNA fragment with the predicted size was obtained by RT-PCR in case 1. In case 2, no products were identified, indicating that the tumor of the patient did not express *MET*. No mutations were identified in case 1 by sequencing. *TFE3* split signals were not observed in either of the 2 cases by FISH.

DISCUSSION

Recently, 2 independent groups have reported vinculin-ALK (VCL-ALK) in renal cancer (Table 1).[35,36] These findings broaden the spectrum of ALK fusion–positive tumors. Interestingly, the 2 patients described in the reports share several uncommon backgrounds for renal cancer: very early onset (6- and 16-year-old boys), a history of sickle cell trait, and uncommon histopathological subtypes (medullary subtype and indeterminate subtype with mixed features of medullary, chromophobe, and transitional cell subtypes). In this study, we screened 355 renal tumors, including 343 RCCs, and identified ALK fusions in 2 RCCs. Significantly, we identified ALK fusions in adult patients (36- and 53-year-old females) without sickle cell trait. This finding will provide a key to ALK inhibitor therapy for more common renal cancers.

RCC associated with *TFE3* gene fusions is already a distinctive entity in the World Health Organization classification,[37,38] and *MET* mutation has been described in 13% of sporadic papillary RCCs.[39] In the present study, we identified neither *MET* nor *TFE3* aberrations in our ALK-positive renal cancer cases. *ALK* rearrangements are recognized as almost mutually exclusive to other mutations such as *EGFR* (epidermal growth factor receptor) and *KRAS* (v-Ki-ras2 Kirsten rat sarcoma viral oncogene) in lung cancer.[6,40] All of the tumor cells in the 2 ALK-positive renal cancers observed by immunohistochemistry expressed ALK fusion protein, suggesting that all tumor cells harbor one or more *ALK* fusion genes. Therefore, as well as other ALK-positive tumors, *ALK* rearrangement in renal cancer probably occurs at a very early phase of carcinogenesis, and is likely to be a driver mutation and mutually exclusive to other driver mutations. As in the case of ALK-positive ALCL, ALK-positive renal cancer will be a distinct molecular pathological entity.

TPM3-ALK was first identified in ALCL in 1999,[41] and subsequently found in IMT in 2000.[5] Therefore, RCC is the third type of cancer that may harbor TPM3-ALK. The organ distribution of EML4-ALK is somewhat controversial. Since its discovery, EML4-ALK has been reported to be identified in lung, breast, and colon cancers. Many research groups have reported the presence of EML4-ALK in a small subset of lung adenocarcinomas (2%-10%). Interestingly, a group in the United States reported the presence of EML4-ALK in breast (5 of 209) and colorectal (2 of 83) cancers, identified by RT-PCR optimized for variants 1, 2, and 3, without showing histopathological evidence.[42] In contrast, 2 Japanese groups examined these cancers (90 breast and 96 colon cancers by RT-PCR for EML4-ALK variants 1 and 2, and 48 breast and 50 colon cancers by multiplex RT-PCR for all possible fusions), but detected no positive cases.[30,43] One possible reason for this discrepancy may be differences in ethnicity. In the present study, we showed histopathological features of the 2 ALK-positive renal cancers. In addition to morphology, the positivity of PAX2 and PAX8 and the negativity of TTF1 strongly indicated that the ALK-positive cancers of the present cases were primary RCCs, and not metastatic lesions of ALK-positive lung cancer.

The oncogenic activities of TPM3-ALK and EML4-ALK have previously been documented,[30,44] and therefore we did not demonstrate them in the present study. As in the case of other ALK-positive tumors, ALK-positive renal cancer is a promising candidate disease for ALK inhibitor therapy. In the present study, we screened surgically removable cases; the prognoses for the 2 ALK-positive patients were good, without recurrence. To realize the full potential of ALK inhibitors in renal cancers, it is important to identify the detailed clinicopathological features of ALK-positive cases, especially those of advanced or recurrent cases, by large-scale screening. For this purpose, anti-ALK immunohistochemistry can most readily be carried out as a primary screening tool. However, caution is needed; the screening immunohistochemical assay should be appropriately sensitive, because our present findings indicate that renal cancer involves EML4-ALK, which is barely detectable by conventional immunohistochemistry methods.[13,45]

Is morphology a clue to the presence of ALK fusion in renal cancers? Almost all ALK-positive lung cancers are adenocarcinomas, and more frequently show mucinous cribriform patterns and signet-ring cells than do ALK-negative adenocarcinomas.[18,31,46] ALK fusion is probably very rare in clear cell RCC, which is the most common

Table 1. ALK-Positive Renal Cancers: Present Cases and Review of Literature

Characteristic	VCL-ALK (Debelenko et al[36])	VCL-ALK (Marino-Enriquez et al[35])	TPM3-ALK (Case 1)	EML4-ALK (Case 2)
Age, y	16	6	36	53
Sex	Male	Male	Female	Female
Ethnicity	African American	African American	Japanese	Japanese
Past history	Sickle cell trait	Sickle cell trait	Tuberculosis (22 y old)	Pleomorphic adenoma (50 y old)
Karyotype	Abnormal complex karyotype	46,XY,t(2;10)(p23;q22), add(14)(p11)	Not examined	Not examined
Symptom	Right flank pain, gross hematuria	Intermittent periumbilical pain, hematuria	Pyelonephritis	Microscopic hematuria
Stage	Stage III	Stage I	Stage I	Stage I
Follow-up	9 mo, alive. No evidence of disease	21 mo, alive. No evidence of disease	2 y, alive. No evidence of disease	3 y, alive. No evidence of disease
Gross findings	6.5-cm irregularly shaped solid tumor mass with infiltrative borders centered in the right renal medulla	4.5-cm irregularly spherical mass with lobulated, fleshy light tan appearance centered in the medulla	4.0 cm × 4.0 cm × 3.5 cm irregularly shaped solid tumor with expansive borders centered in the cortex	Double cancer. A: 2.5 cm × 2.5 cm ×2.3 cm solid yellow tumor in the cortex of the left intermediate pole. B: 0.6-cm yellow mass in the cortex of the left inferior pole
Microscopic findings	Diffuse sheet-like pattern; round, oval, and polygonal tumor cells; eosinophilic cytoplasm; moderately polymorphic and vesicular nuclei	Solid growth pattern; spindle-shaped cells with large vesicular nuclei; clear coarse chromatin and abundant eosinophilic cytoplasm	Papillary, tubular, or cribriform growth of cuboidal cells with eosinophilic cytoplasm. Nuclei round to ovoid; nuclear size basically uniform	A: Papillary structure of cuboidal or low columnar cells with eosinophilic cytoplasm and small uniform round to oval nuclei. B: Clear cell
Immunohistochemistry	Positive: AE1/AE3, CAM5.2, CK7, EMA, INI1, TFE3. Negative: CD10, S100, HMB45, WT1	Positive: AE1/AE3, CAM5.2, EMA	Positive: ALK, vimentin, EMA, cytokeratin 7, AE1/AE3, CAM5.2, 34βE12, AMACR (focal), CD10 (focal), PAX2 (focal), PAX8 (focal). Negative: TTF1, RCC Ma	A: Positive: ALK, vimentin, EMA, cytokeratin 7, AE1/AE3, CAM5.2, 34βE12, AMACR (focal), PAX2 (focal), PAX8 (focal). Negative: CD10, TTF1, RCC Ma
Diagnosis	Renal cell carcinoma, indeterminate subtype (medullary, chromophobe, transitional cell carcinoma mixed)	Renal medullary carcinoma	Renal cell carcinoma, unclassified	A: Papillary renal cell carcinoma, type 2A. B: Clear cell renal cell carcinoma

ALK indicates anaplastic lymphoma kinase; EML4, echinoderm microtubule–associated protein like 4; TPM3, tropomyosin 3; VCL, vinculin.

subtype of renal cancer; 2 previously reported cases with VCL-ALK were not clear cell RCC,[35,36] and we identified no ALK-positive cases in 255 clear cell RCCs in this study. Interestingly, case 1 showed a mucinous cribriform pattern. This may be a characteristic feature of ALK-positive carcinomas, universally applicable to carcinomas of various organs. Further study with a larger number of cases is warranted.

Molecular-targeted therapy of advanced renal cancers is starting to realize its full potential. However, complete remission is rarely achieved, because no agent targets a key molecule associated with "oncogene addiction" of renal cancer. In this context, ALK fusion constitutes a promising advance in renal cancers, as has previously been demonstrated with various other types of cancer. In the present study, we identified 2 adult cases of ALK-positive renal cancer in patients without uncommon backgrounds. Our findings confirm the potential of ALK inhibitor therapy for RCC. More detailed clinicopathological features of ALK-positive renal cancers, especially at higher clinical stages, are desirable. Hunting the "ALKoma" in various types of carcinomas, as well as in lung and kidney cancer, will provide an answer to these pathological and clinical questions.

CONFLICT OF INTEREST DISCLOSURE

Dr. Takeuchi is a scientific advisor for the anti-ALK iAEP immunohistochemistry kit (ALK Detection Kit, Nichirei Bioscience, Tokyo, Japan). All remaining authors have made no disclosures.

REFERENCES

1. International Agency for Research on Cancer. The GLOBOCAN Project: GLOBOCAN 2008. http://globocan.iarc.fr/. Accessed December 16, 2011.
2. Campbell SC, Novick AC, Bukowski RM. Renal tumors. In: Wein AJ, Kavoussi LR, Novick AC, Partin AW, Peters CA, eds. Campbell-Walsh Urology. 9th ed. Philadelphia, PA: Saunders; 2007: 1567-1637.
3. Morris SW, Kirstein MN, Valentine MB, et al. Fusion of a kinase gene, ALK, to a nucleolar protein gene, NPM, in non-Hodgkin's lymphoma. Science. 1994;263:1281-1284.
4. Shiota M, Fujimoto J, Semba T, Satoh H, Yamamoto T, Mori S. Hyperphosphorylation of a novel 80 kDa protein-tyrosine kinase similar to Ltk in a human Ki-1 lymphoma cell line, AMS3. Oncogene. 1994;9:1567-1574.
5. Lawrence B, Perez-Atayde A, Hibbard MK, et al. TPM3-ALK and TPM4-ALK oncogenes in inflammatory myofibroblastic tumors. Am J Pathol. 2000;157:377-384.
6. Soda M, Choi YL, Enomoto M, et al. Identification of the transforming EML4-ALK fusion gene in non-small-cell lung cancer. Nature. 2007;448:561-566.
7. Rikova K, Guo A, Zeng Q, et al. Global survey of phosphotyrosine signaling identifies oncogenic kinases in lung cancer. Cell. 2007; 131:1190-1203.
8. Soda M, Takada S, Takeuchi K, et al. A mouse model for EML4-ALK-positive lung cancer. Proc Natl Acad Sci U S A. 2008;105: 19893-19897.
9. Kwak EL, Bang YJ, Camidge DR, et al. Anaplastic lymphoma kinase inhibition in non-small-cell lung cancer. N Engl J Med. 2010;363:1693-1703.
10. Chihara D, Suzuki R. More on crizotinib. N Engl J Med. 2011;364: 776-777.
11. Butrynski JE, D'Adamo DR, Hornick JL, et al. Crizotinib in ALK-rearranged inflammatory myofibroblastic tumor. N Engl J Med. 2010;363:1727-1733.
12. Gambacorti-Passerini C, Messa C, Pogliani EM. Crizotinib in anaplastic large-cell lymphoma. N Engl J Med. 2011;364:775-776.
13. Takeuchi K, Choi YL, Togashi Y, et al. KIF5B-ALK, a novel fusion oncokinase identified by an immunohistochemistry-based diagnostic system for ALK-positive lung cancer. Clin Cancer Res. 2009;15: 3143-3149.
14. Martelli MP, Sozzi G, Hernandez L, et al. EML4-ALK rearrangement in non-small cell lung cancer and non-tumor lung tissues. Am J Pathol. 2009;174:661-670.
15. Jokoji R, Yamasaki T, Minami S, et al. Combination of morphological feature analysis and immunohistochemistry is useful for screening of EML4-ALK-positive lung adenocarcinoma. J Clin Pathol. 2010;63:1066-1070.
16. Kijima T, Takeuchi K, Tetsumoto S, et al. Favorable response to crizotinib in three patients with echinoderm microtubule-associated protein-like 4-anaplastic lymphoma kinase fusion-type oncogene-positive non-small cell lung cancer. Cancer Sci. 2011;102:1602-1604.
17. Kimura H, Nakajima T, Takeuchi K, et al. ALK fusion gene positive lung cancer and 3 cases treated with an inhibitor for ALK kinase activity. Lung Cancer. 2012;75:66-72.
18. Yoshida A, Tsuta K, Nakamura H, et al. Comprehensive histologic analysis of ALK-rearranged lung carcinomas. Am J Surg Pathol. 2011;35:1226-1234.
19. Yi ES, Boland JM, Maleszewski JJ, et al. Correlation of IHC and FISH for ALK gene rearrangement in non-small cell lung carcinoma: IHC score algorithm for FISH. J Thorac Oncol. 2011;6:459-465.
20. Kudo K, Takeuchi K, Tanaka H, et al. Immunohistochemical screening of ALK lung cancer with biopsy specimens of advanced lung cancer. J Clin Oncol. 2010;28(suppl): (abstract 10532).
21. Sakairi Y, Nakajima T, Yasufuku K, et al. EML4-ALK fusion gene assessment using metastatic lymph node samples obtained by endobronchial ultrasound-guided transbronchial needle aspiration. Clin Cancer Res. 2010;16:4938-4945.
22. Nakajima T, Kimura H, Takeuchi K, et al. Treatment of lung cancer with an ALK Inhibitor after EML4-ALK fusion gene detection using endobronchial ultrasound-guided transbronchial needle aspiration. J Thorac Oncol. 2010;5:2041-2043.
23. Takeuchi K, Soda M, Togashi Y, et al. Identification of a novel fusion, SQSTM1-ALK, in ALK-positive large B-cell lymphoma. Haematologica. 2011;96:464-467.
24. Takeuchi K, Soda M, Togashi Y, et al. Pulmonary inflammatory myofibroblastic tumor expressing a novel fusion, PPFIBP1-ALK: reappraisal of anti-ALK immunohistochemistry as a tool for novel ALK-fusion identification. Clin Cancer Res. 2011;17:3341-3348.
25. Shiota M, Fujimoto J, Takenaga M, et al. Diagnosis of t(2;5)(p23;q35)-associated Ki-1 lymphoma with immunohistochemistry. Blood. 1994;84:3648-3652.
26. Pulford K, Lamant L, Morris SW, et al. Detection of anaplastic lymphoma kinase (ALK) and nucleolar protein nucleophosmin (NPM)-ALK proteins in normal and neoplastic cells with the monoclonal antibody ALK1. Blood. 1997;89:1394-1404.
27. Shiota M, Nakamura S, Ichinohasama R, et al. Anaplastic large cell lymphomas expressing the novel chimeric protein p80NPM/ALK: a distinct clinicopathologic entity. Blood. 1995;86:1954-1960.
28. Delsol G, Lamant L, Mariamé B, et al. A new subtype of large B-cell lymphoma expressing the ALK kinase and lacking the 2; 5 translocation. Blood. 1997;89:1483-1490.
29. Lamant L, Pulford K, Bischof D, et al. Expression of the ALK tyrosine kinase gene in neuroblastoma. Am J Pathol. 2000;156:1711-1721.
30. Takeuchi K, Choi YL, Soda M, et al. Multiplex reverse transcription-PCR screening for EML4-ALK fusion transcripts. Clin Cancer Res. 2008;14:6618-6624.
31. Inamura K, Takeuchi K, Togashi Y, et al. EML4-ALK fusion is linked to histological characteristics in a subset of lung cancers. J Thorac Oncol. 2008;3:13-17.
32. Lopez-Beltran A, Carrasco JC, Cheng L, Scarpelli M, Kirkali Z, Montironi R. 2009 update on the classification of renal epithelial tumors in adults. Int J Urol. 2009;16:432-443.
33. Delahunt B, Eble JN. Papillary renal cell carcinoma: a clinicopathologic and immunohistochemical study of 105 tumors. Mod Pathol. 1997;10:537-544.
34. Yang XJ, Tan MH, Kim HL, et al. A molecular classification of papillary renal cell carcinoma. Cancer Res. 2005;65:5628-5637.
35. Mariño-Enríquez A, Ou WB, Weldon CB, Fletcher JA, Pérez-Atayde AR. ALK rearrangement in sickle cell trait-associated renal medullary carcinoma. Genes Chromosomes Cancer. 2011;50:146-153.
36. Debelenko LV, Raimondi SC, Daw N, et al. Renal cell carcinoma with novel VCL-ALK fusion: new representative of ALK-associated tumor spectrum. Mod Pathol. 2011;24:430-442.
37. Argani P, Ladanyi M. Renal carcinomas associated with Xp11.2 translocations/TFE3 gene fusions. In: Eble J, Sauter G, Epstein J, Sesterhenn I, eds. Pathology and Genetics of Tumours of the Urinary System and Male Genital Organs. Lyon, France: IARC Press; 2004:37-38.
38. Ross H, Argani P. Xp11 translocation renal cell carcinoma. Pathology. 2010;42:369-373.

39. Schmidt L, Junker K, Nakaigawa N, et al. Novel mutations of the MET proto-oncogene in papillary renal carcinomas. *Oncogene.* 1999; 18:2343-2350.

40. Inamura K, Takeuchi K, Togashi Y, et al. EML4-ALK lung cancers are characterized by rare other mutations, a TTF-1 cell lineage, an acinar histology, and young onset. *Mod Pathol.* 2009;22:508-515.

41. Lamant L, Dastugue N, Pulford K, Delsol G, Mariamé B. A new fusion gene TPM3-ALK in anaplastic large cell lymphoma created by a (1;2)(q25;p23) translocation. *Blood.* 1999;93: 3088-3095.

42. Lin E, Li L, Guan Y, et al. Exon array profiling detects EML4-ALK fusion in breast, colorectal, and non-small cell lung cancers. *Mol Cancer Res.* 2009;7:1466-1476.

43. Fukuyoshi Y, Inoue H, Kita Y, Utsunomiya T, Ishida T, Mori M. EML4-ALK fusion transcript is not found in gastrointestinal and breast cancers. *Br J Cancer.* 2008;98:1536-1539.

44. Giuriato S, Faumont N, Bousquet E, et al. Development of a conditional bioluminescent transplant model for TPM3-ALK-induced tumorigenesis as a tool to validate ALK-dependent cancer targeted therapy. *Cancer Biol Ther.* 2007;6:1318-1323.

45. Sozzi G, Martelli MP, Conte D, et al. The EML4-ALK transcript but not the fusion protein can be expressed in reactive and neoplastic lymphoid tissues. *Haematologica.* 2009;94:1307-1311.

46. Rodig SJ, Mino-Kenudson M, Dacic S, et al. Unique clinicopathologic features characterize ALK-rearranged lung adenocarcinoma in the western population. *Clin Cancer Res.* 2009;15:5216-5223.

Clinical Cancer Research

ЯICꞱ

A Prospective PCR-Based Screening for the *EML4-ALK* Oncogene in Non -Small Cell Lung Cancer

Manabu Soda, Kazutoshi Isobe, Akira Inoue, et al.

Updated Version	Access the most recent version of this article at: doi:10.1158/1078-0432.CCR-11-2947
Supplementary Material	Access the most recent supplemental material at: http://clincancerres.aacrjournals.org/content/suppl/2012/08/20/1078-0432.CCR-11-2947.DC1.html

Cited Articles	This article cites 29 articles, 16 of which you can access for free at: http://clincancerres.aacrjournals.org/content/18/20/5682.full.html#ref-list-1

E-mail alerts	Sign up to receive free email-alerts related to this article or journal.
Reprints and Subscriptions	To order reprints of this article or to subscribe to the journal, contact the AACR Publications Department at pubs@aacr.org.
Permissions	To request permission to re-use all or part of this article, contact the AACR Publications Department at permissions@aacr.org.

Clinical
Cancer
Research

A Prospective PCR-Based Screening for the *EML4-ALK* Oncogene in Non–Small Cell Lung Cancer

Manabu Soda[1], Kazutoshi Isobe[2], Akira Inoue[6], Makoto Maemondo[7], Satoshi Oizumi[8], Yuka Fujita[9], Akihiko Gemma[3], Yoshihiro Yamashita[1], Toshihide Ueno[1], Kengo Takeuchi[4], Young Lim Choi[1,5], Hitoshi Miyazawa[10], Tomoaki Tanaka[10], Koichi Hagiwara[10], and Hiroyuki Mano[1,5,11], for the North-East Japan Study Group and the ALK Lung Cancer Study Group

Abstract

Purpose: *EML4-ALK* is a lung cancer oncogene, and ALK inhibitors show marked therapeutic efficacy for tumors harboring this fusion gene. It remains unsettled, however, how the fusion gene should be detected in specimens other than formalin-fixed, paraffin-embedded tissue. We here tested whether reverse transcription PCR (RT-PCR)-based detection of *EML4-ALK* is a sensitive and reliable approach.

Experimental Design: We developed a multiplex RT-PCR system to capture *ALK* fusion transcripts and applied this technique to our prospective, nationwide cohort of non–small cell lung cancer (NSCLC) in Japan.

Results: During February to December 2009, we collected 916 specimens from 853 patients, quality filtering of which yielded 808 specimens of primary NSCLC from 754 individuals. Screening for *EML4-ALK* and *KIF5B-ALK* with our RT-PCR system identified *EML4-ALK* transcripts in 36 samples (4.46%) from 32 individuals (4.24%). The RT-PCR products were detected in specimens including bronchial washing fluid ($n = 11$), tumor biopsy ($n = 8$), resected tumor ($n = 7$), pleural effusion ($n = 5$), sputum ($n = 4$), and metastatic lymph node ($n = 1$). The results of RT-PCR were concordant with those of sensitive immuno-histochemistry with ALK antibodies.

Conclusions: Multiplex RT-PCR was confirmed to be a reliable technique for detection of *ALK* fusion transcripts. We propose that diagnostic tools for *EML4-ALK* should be selected in a manner dependent on the available specimen types. FISH and sensitive immunohistochemistry should be applied to formalin-fixed, paraffin-embedded tissue, but multiplex RT-PCR is appropriate for other specimen types. *Clin Cancer Res; 18(20); 5682–9. ©2012 AACR.*

Introduction

An oncogenic fusion between the echinoderm microtubule-associated protein–like 4 gene (*EML4*) and the ana-

Authors' Affiliations: [1]Division of Functional Genomics, Jichi Medical University, Tochigi; [2]Department of Respiratory Medicine, Toho University Omori Medical Center; [3]Nippon Medical School Hospital; [4]Pathology Project for Molecular Targets, The Cancer Institute; [5]Department of Medical Genomics, Graduate School of Medicine, University of Tokyo, Tokyo; [6]Tohoku University Hospital; [7]Miyagi Cancer Center, Miyagi; [8]First Department of Medicine, Hokkaido University School of Medicine; [9]Asahikawa Medical Center, Hokkaido; [10]Saitama Medical University Hospital; and [11]CREST, Japan Science and Technology Agency, Saitama, Japan

Corresponding Author: Hiroyuki Mano, Division of Functional Genomics, Jichi Medical University, 3311-1 Yakushiji, Shimotsukeshi, Tochigi 329-0498, Japan. Phone: 81-285-58-7449; Fax: 81-285-44-7322; E-mail: hmano@jichi.ac.jp

plastic lymphoma kinase gene (*ALK*) was discovered by functional screening with a non–small cell lung cancer (NSCLC) specimen (1). *EML4* and *ALK* are located within a short distance (~12 Mbp) of each other on the short arm of human chromosome 2, and a small inversion involving the 2 loci is responsible for generation of the *EML4-ALK* fusion in lung cancer. The EML4-ALK tyrosine kinase undergoes constitutive dimerization through a coiled-coil domain within EML4, resulting in kinase activation and conferring potent transforming ability (2, 3). Transgenic mice expressing *EML4-ALK* in lung alveolar cells develop multiple adenocarcinoma nodules soon after birth, but treatment with an ALK inhibitor results in the rapid clearance of such nodules, confirming the addiction of EML4-ALK–positive tumors to the kinase activity of the fusion protein (4). The therapeutic efficacy of ALK inhibitors has been confirmed in other transgenic mice expressing EML4-ALK (5).

Several ALK inhibitors have already entered clinical trials or are under preclinical development (6–10). Marked therapeutic efficacy of one such compound, crizotinib, has been described in patients with NSCLCs positive for *EML4-ALK*, with an overall response rate of 57% (7), and crizotinib was recently approved as a therapeutic drug by the U.S. Food

American Association for Cancer Research

— 66 —

Translational Relevance

The recent approval of an ALK inhibitor by the U.S. Food and Drug Administration has rendered urgent the development of a diagnostic scheme for tumors harboring *ALK* fusion genes. Whereas FISH is effective for analysis of formalin-fixed, paraffin-embedded (FFPE) tissue, how to test other types of specimen remains unsettled. We conducted a prospective, nationwide screening for *EML4-ALK*- or *KIF5B-ALK*-positive lung carcinomas in Japan with the use of a newly developed multiplex reverse transcription (RT)-PCR system. Various subtypes of *EML4-ALK* cDNA were identified in 36 of 808 specimens with adequate RNA quality. The RT-PCR results were concordant with those of immunohistochemistry, and *EML4-ALK* PCR products were detected in independent specimens from the same individuals. As far as we are aware, our study represents the first prospective RT-PCR–based screening for *EML4-ALK*, and it shows that multiplex RT-PCR is reliable for detection of the fusion gene in non-FFPE specimens.

and Drug Administration within a remarkably short period after target discovery (3, 11).

The failure of crizotinib treatment in individuals without oncogenic *ALK* fusions (12) and an adverse effect of treatment with gefitinib on the prognosis of patients with NSCLCs who do not harbor mutations of the EGF receptor (*EGFR*) gene (13) both suggest that ALK inhibitors should be administered only to patients positive for oncogenic ALK proteins. FISH-based detection of *ALK* rearrangements has proved to be of diagnostic use in the trials with crizotinib (7). Furthermore, detection of ALK proteins by sensitive immunohistochemistry (IHC) has been described (14, 15), and one such immunohistochemical screening approach resulted in the identification of another oncogenic ALK fusion, KIF5B-ALK (14). However, a substantial proportion of patients attending clinics are diagnosed with lung cancer on the basis of pathologic analysis of bronchial lavage fluid, pleural effusion, or sputum. Given that these specimens are not always suitable for the preparation of formalin-fixed, paraffin-embedded (FFPE) tissue required for FISH or IHC, individuals who are diagnosed solely by analysis of such specimens cannot receive EML4-ALK tests. To allow the sensitive detection of *EML4-ALK* and *KIF5B-ALK* in such specimens, we have now developed a multiplex reverse transcription (RT)-PCR system that captures the 2 *ALK* fusions, and we have tested its reliability as a diagnostic tool in our large-scale prospective cohort.

Materials and Methods

Prospective collection of NSCLC specimens

During February to December of 2009, we collected a total of 916 lung cancer specimens from 853 independent patients through our multicenter, nationwide networks in Japan. All specimens but resected tumors were mixed with

RLT buffer (Qiagen) immediately after sampling, a step that markedly inhibits RNA degradation for up to 3 days at room temperature (data not shown). Resected tumor samples were snap-frozen and stored at $-80°C$ until extraction of RNA and DNA. Portions of the samples were sent to Jichi Medical University (Tochigi, Japan) for multiplex RT-PCR analysis of *EML4-ALK* and *KIF5B-ALK* fusions and to Saitama Medical University (Saitama, Japan) for peptide nucleic acid–locked nucleic acid (PNA-LNA) PCR clamp analysis of *EGFR* mutations (16). All specimens were confirmed by pathologic analysis to contain malignant cells. More than half of the specimens were collected through the North-East Japan Study Group network according to the NEJ004 protocol. The study was approved by the Institutional Review Board of each participating center, and written informed consent was obtained from each study subject. All statistical analysis was conducted with 2-sided tests, and a $P < 0.05$ was considered statistically significant.

Clinicopathologic features of EML4-ALK–positive NSCLC

The clinicopathologic features of patients with *EML4-ALK*–positive or -negative tumors in our cohort are summarized in Table 1 and Supplementary Table S1. Consistent with previous observations, *EML4-ALK*–positive patients were significantly younger than those without *EML4-ALK* ($P < 0.001$, Student' t test) and were enriched in never or light smokers ($P < 0.001$, Fisher exact test). Our data also indicated that *EML4-ALK*–positive tumors are more likely to occur in women than in men ($P < 0.001$, Fisher exact test). In the present cohort, *EML4-ALK* was detected only in lung adenocarcinoma ($P < 0.001$, Fisher exact test), for which the fusion-positive rate was 6.11%.

A total of 718 specimens were screened for *EGFR* mutations, with such mutations being detected in 171 cases (23.8%). Whereas most *EML4-ALK*–positive tumors did not harbor *EGFR* mutations ($P = 0.002$, Fisher exact test), we did detect one tumor doubly positive in this regard. *EML4-ALK* and *EGFR* mutations are largely mutually exclusive (17, 18), but, importantly, such exclusiveness may not be absolute (19). Given that the presence of *EML4-ALK* and *EGFR* mutations in our doubly positive patient was examined with cells isolated from bronchial washing fluid, which was the only available specimen for molecular analysis in this individual, we were not able to determine whether there was a genuinely double-positive tumor in the lung or there were multiple independent tumors each positive for *EML4-ALK* or mutated *EGFR*.

We also attempted to examine the mutation status of *KRAS* among our 32 cases positive for *EML4-ALK*. We were able to sequence *KRAS* cDNAs for 26 of these patients, none of whom showed *KRAS* alterations (data not shown), confirming the mutual exclusivity of *EML4-ALK* and *KRAS* mutations (17, 20, 21).

Quality assessment of samples

Complementary DNA prepared from the specimens was first subjected to RT-PCR analysis with primers (5'-

— 67 —

Table 1. Characteristics of subjects positive for *EML4-ALK* by the RT-PCR diagnostic system.

Identification number	Sex/ age, y	Pathologic classification	Specimen type	EML4-ALK variant	Smoking history (pack-years)	TNM classification	Clinical stage	iAEP	EGFR mutation	KRAS mutation
J-#1	M/27	Adenocarcinoma	Sputum (2 different time points)	E13;A20	0	cT4N3M1	4	+	−	−
J-#4	F/39	Adenocarcinoma	Metastatic lymph node	E20;A20	NA	cTxN3M1	4	+	−	−
J-#7	M/74	Adenocarcinoma	Bronchial washing fluid	E13;A20	50	cT4N3M1	4	ND	−	−
J-#12	F/56	Adenocarcinoma	Resected tumor	E13;A20	0	cT1N0M0	1A	+	−	ND
J-#53	M/48	Adenocarcinoma	Tumor biopsy/sputum	E13;A20	0	cT3N2M1	4	+	−	−
J-#88	F/37	Adenocarcinoma	Pleural effusion	E13;A20	0	cT4N3M1	4	ND	−	−
J-#127	F/49	Adenocarcinoma	Tumor biopsy	E6a/b;A20	0.9	cT1N2M1	4	+	−	−
J-#189	F/37	Adenocarcinoma	Resected tumor	E14::ins2; ins56A20	0	cT2N1M1	4	+	−	−
J-#210	F/37	Adenocarcinoma	Resected tumor	E13;A20	0	cT4N2M1	4	ND	−	−
J-#215	F/61	Adenocarcinoma	Sputum	E13;A20	82	cT4N2M1	4	ND	−	−
J-#330	M/72	Adenocarcinoma	Pleural effusion/resected tumor (2 different regions)	E13;A20	0	cT4N1M1	4	+	−	−
J-#350	F/53	Adenocarcinoma	Pleural effusion	E13;A20	0	cT4N2M0	3B	ND	−	−
J-#378	F/78	Adenocarcinoma	Resected tumor	E13;A20	0	cT1N0M0	1A	ND	−	−
J-#385	F/80	Adenocarcinoma	Pleural effusion	E6a/b;A20	0	cT4N3M1	4	ND	−	−
J-#391	F/55	Adenocarcinoma	Tumor biopsy	E13;A20	16.5	cT2N2M1	4	+	−	ND
J-#392	F/38	Adenocarcinoma	Tumor biopsy	E13;A20	34	cT4N2M0	3B	+	−	ND
J-#393	F/42	Adenocarcinoma	Tumor biopsy	E13;A20	0	cT4N3M1	4	−	−	ND
J-#409	F/35	Adenocarcinoma	Tumor biopsy	E13;A20	0	cT4N0M0	3B	+	−	−
J-#422	M/69	Adenocarcinoma	Tumor biopsy	E6a/b;A20	0	cT2N2M0	3A	ND	−	−
J-#450	F/30	Adenocarcinoma	Bronchial washing fluid	E6a/b;A20	0	cT4N2M1	4	+	−	−
J-#530	F/55	Adenocarcinoma	Bronchial washing fluid	E13;A20	0	cT1N1M1	4	+	+	ND
J-#646	F/36	Adenocarcinoma	Bronchial washing fluid	E6a/b;A20	0	cT2N3M0	3B	ND	−	−
J-#657	F/62	Adenocarcinoma	Bronchial washing fluid	E13;A20	15	cT4N2M0	3B	ND	−	−
J-#759	F/32	Adenocarcinoma	Resected tumor	E13;A20	12	cT1N0M0	1A	ND	−	−
J-#771	M/32	Adenocarcinoma	Tumor biopsy	E6a/b;A20	15	cT1N3M1	3B	ND	−	−
J-#817	M/33	Adenocarcinoma	Pleural effusion	E13;A20	0	cT2N1M1	4	ND	−	−
J-#848	M/57	Adenocarcinoma	Bronchial washing fluid	E18;E20	0	cT4N2M0	3B	ND	−	−
J-#887	F/32	Adenocarcinoma	Bronchial washing fluid	E6a/b;A20	0	cTxN3M1	4	ND	−	ND
J-#927	M/36	Adenocarcinoma	Bronchial washing fluid	E6a/b;A20	30	cT4N3M1	4	−	−	−
J-#928	F/71	Adenocarcinoma	Bronchial washing fluid	E6a/b;A20	0	cT4N3M1	4	ND	−	−
J-#996	M/52	Adenocarcinoma	Bronchial washing fluid	E6a/b;A20	0	cT3N3M0	3B	ND	−	−
J-#1001	F/32	Adenocarcinoma	Bronchial washing fluid	E13;A20	6.5	cT2N2M1	4	+	−	−

Abbreviations: F, female; M, male; NA, not available; ND, not determined.

CTGTGGAGGCTGAACTGGATC-3′ and 5′-TCATCAACAA-GCTCCACGGTG-3′) specific for the human ribonuclease P (RNase P) gene (GenBank accession number NM_005837). Given that we previously showed that the abundance of RNase P mRNA is similar to that of *EML4-ALK* mRNA in NSCLCs (data not shown), we used the successful amplification of RT-PCR products for RNase P as a threshold for selection of specimens for further analysis. Exclusion of small cell lung cancer specimens and filtering on the basis of RNase P mRNA abundance resulted in the isolation of 808 specimens of primary NSCLCs obtained from 754 individuals.

As shown in Supplementary Fig. S1, bronchial washing fluid, including bronchoalveolar lavage fluid and washing fluid for the brush, needle, forceps, and other implements used in bronchoscopy, constituted 66.3% of the 808 eligible samples, with the remaining specimens including pleural effusion (12.8%); surgically resected tumor (7.05%); sputum (4.33%); tumor biopsy tissue including that obtained by transbronchial lung biopsy and transbronchial needle aspiration (3.71%); peripheral blood (3.71%); cardiac effusion, spinal fluid, or ascites (1.36%); and metastatic lesions of NSCLCs (0.74%).

Multiplex RT-PCR analysis of EML4-ALK and KIF5B-ALK

Each specimen (with the exception of resected tumors) was mixed with an equal volume of RLT buffer at the Institute at which it was harvested. The resulting mixture was sent to Jichi Medical University, where DNA and RNA were extracted with the use of an automated BioRobot EZ1 workstation (Qiagen). The isolated RNA was subjected to RT with a ReverTra Ace qPCR RT kit (Toyobo), and the resulting cDNA was subjected to PCR for 50 cycles of incubation at 94°C for 15 seconds, 60°C for 30 seconds, and 72°C for 1 minute with AmpliTAQ Gold DNA polymerase (Applied Biosystems) and with 2 μmol/L of each of the following

− 68 −

primers: F-1, 5'-GCTTTCCCCGCAAGATGGACGG-3'; F-2, 5'-TACCAGTGCTGTCTCAATTGCAGG-3'; F-3, 5'-GTGCA-GTGTTTAGCATTCTTGGGG-3'; F-4, 5'-AGCTACATCACA-CACCTTGACTGG-3'; F-5, 5'-TCAAGCACATCTCAAGAG-CAAGTG-3'; F-6, 5'-ATCCTGCGGAACACTATTCAGTGG-3'; F-7, 5'-GACAGTTGGAGGAATCTGTCGATG-3'; F-8, 5'-CAGCTGAGAGAGTGAAAGCTTTGG-3'; and R-1, 5'-TCTT-GCCAGCAAAGCAGTAGTTGG-3'. All PCR products were subjected to Sanger sequencing to confirm the presence of *EML4-ALK* or *KIF5B-ALK* cDNA.

Results

Multiplex RT-PCR system

In addition to the original *EML4-ALK* fusion cDNA in which exon 13 of *EML4* is fused to exon 20 of *ALK* in an in-frame manner (designated the E13;A20 variant by analogy with karyotype nomenclature; see http://atlasgeneticson-cology.org/Tumors/inv2p21p23NSCCLungID5667.html), 14 different variants of *EML4-ALK* have been described (1, 14, 21–27). Seven exons of *EML4* are theoretically capable of in-frame fusion with exon 20 of *ALK* (Fig. 1A), and all but the E1;A20 variant would be expected to produce an oncogenic EML4-ALK protein, given that the coiled-coil domain encoded by exon 2 is required for constitutive dimerization of EML4-ALK. In addition, 6 different exons of *KIF5B* are theoretically capable of in-frame fusion with exon 20 of *ALK* (Fig. 1A).
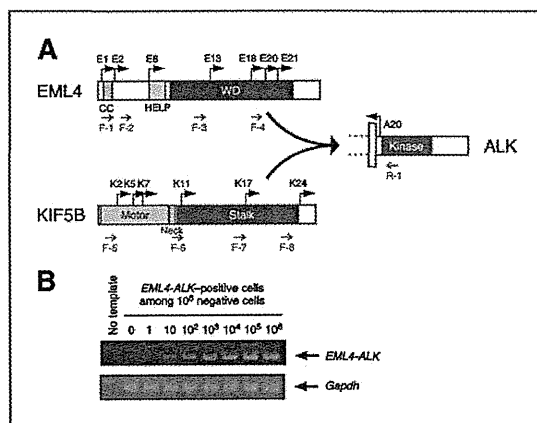

Figure 1. Multiplex RT-PCR system for detection of *EML4-ALK* and *KIF5B-ALK*. A, schematic representation of the structure of EML4, KIF5B, and ALK proteins. The positions of exons (E for *EML4* and K for *KIF5B*) theoretically capable of fusing in-frame to exon 20 (A20) of *ALK* are indicated by arrows. The positions of 8 forward primers (F-1 to F-8) and 1 reverse primer (R-1) for PCR are also indicated below the corresponding proteins. EML4 contains a coiled-coil domain (CC), a hydrophobic EMAP-like protein domain (HELP), and WD repeats (WD). KIF5B consists of an amino-terminal ATP-dependent motor domain, a neck region, and a stalk region. B, various numbers (0 to 1 × 10⁶) of *EML4-ALK* (E13;A20)-positive BA/F3 cells (1) were mixed with a fixed number (1 × 10⁶) of *EML4-ALK*-negative BA/F3 cells, and each mixture was analyzed with our multiplex RT-PCR system. A cDNA for mouse glyceraldehyde-3-phosphate dehydrogenase (*Gapdh*) was also amplified by PCR as an internal control with the primers 5'-TGTGTCCGTCGTGGATCTGA-3' and 5'-CCTGCTTCACCACCTTCTTGA-3'.

To detect any such *EML4-ALK* or *KIF5B-ALK* fusion mRNAs, we developed a multiplex RT-PCR system. We had previously screened our archive of frozen tumors by RT-PCR analysis with 2 forward primers targeted to *EML4* and 1 reverse primer targeted to *ALK* (24), but such PCR conditions resulted in the amplification of products as large as ~1,300 bp for some variants. In this prospective study, we were faced with the analysis of a large number of samples with different levels of RNA quality. If the size of PCR products varied substantially among different *EML4-ALK* or *KIF5B-ALK* variants, some variants with large PCR products might not be amplified efficiently from specimens with low RNA quality. To be able to diagnose all possible fusions even with such samples, we therefore designed 4 forward primers for each of *EML4* and *KIF5B* so that the size variation among all possible RT-PCR products is minimal (Fig. 1A). This new multiplex system faithfully detected all known fusion variants from *EML4-ALK*–positive specimens in our previous archive of NSCLCs (data not shown).

To examine the sensitivity of our RT-PCR system, we mixed *EML4-ALK*–expressing BA/F3 cells (0 to 1 × 10⁶) with *EML4-ALK*–negative cells (1 × 10⁶) and then subjected them to RT-PCR analysis. A fusion cDNA was readily identified even with 10 positive cells (0.001%) among 1 × 10⁶ negative cells (Fig. 1B), showing the high sensitivity of the RT-PCR system.

To confirm the potential of our RT-PCR–based system, we compared it with a sensitive immunohistochemical approach and with FISH for the diagnosis of our archive of surgically resected and freshly frozen tumors with high RNA quality. Fifteen NSCLC specimens that previously stained positive by our sensitive immunohistochemical approach, which is based on an intercalated antibody-enhanced polymer (iAEP) method (14), were analyzed by RT-PCR and FISH together with 96 iAEP-negative specimens in a blinded manner. RT-PCR analysis of all these specimens ($n = 111$) yielded a diagnosis identical to that obtained with the iAEP method ($P = 7.3 \times 10^{-19}$, Fisher exact test; data not shown). Analysis of the same sample set by a split FISH assay with Vysis probes (Abbott Laboratories) revealed that all of the iAEP-positive cases showed a rearranged *ALK* locus, whereas one iAEP-negative sample gave a discordant result (negative by iAEP and RT-PCR but positive by FISH; Supplementary Fig. S2). The reason for this discrepant result remains unclear, but the multiple signals obtained with the 3'-*ALK* probe in the FISH analysis are indicative of amplification of the *ALK* gene or its adjacent region. Despite this discrepancy, the RT-PCR and iAEP data were highly concordant with the FISH results ($P = 1.2 \times 10^{-17}$, Fisher exact test). Compared with the iAEP method, therefore, both the sensitivity and specificity of our RT-PCR system were 100%. In comparison with the Vysis FISH, the sensitivity and specificity of RT-PCR were 93.8% and 100%, respectively.

Detection of EML4-ALK

Screening of the 808 eligible specimens with our multiplex RT-PCR system identified positive products in 36 samples (4.46%) obtained from 32 different individuals
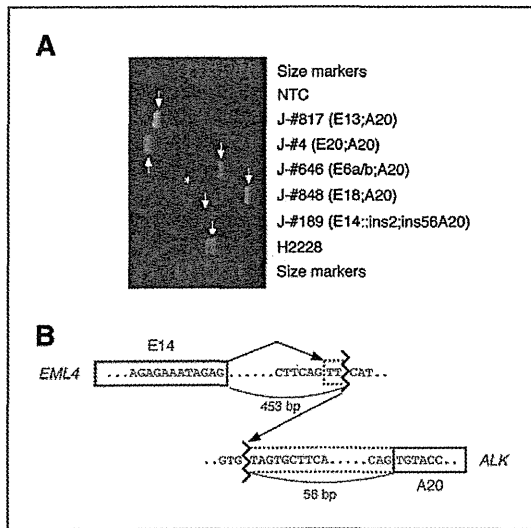
— 69 —

Figure 2. Multiplex RT-PCR detection of *EML4-ALK*–positive NSCLCs. A, RT-PCR products for each of the *EML4-ALK* variants identified in our cohort were separated by agarose gel electrophoresis. RT-PCR products spanning the *EML4-ALK* fusion points are indicated by arrows; the asterisk indicates a nonspecific product. An NSCLC cell line, H2228, harboring the E6a/b;A20 variant of *EML4-ALK* was used as a positive control for the PCR reaction. Size markers include a 50-bp DNA ladder (Invitrogen). NTC, no-template control. B, genomic structure of the fusion point for a novel variant of *EML4-ALK*. Nucleotide sequencing of the genomic PCR and RT-PCR products from patient J-#189 revealed that exon 14 of *EML4* (blue) was spliced to a TT sequence adjacent to the genomic ligation point, with transcription continuing in an in-frame manner into intron 19 and exon 20 of *ALK* (red).
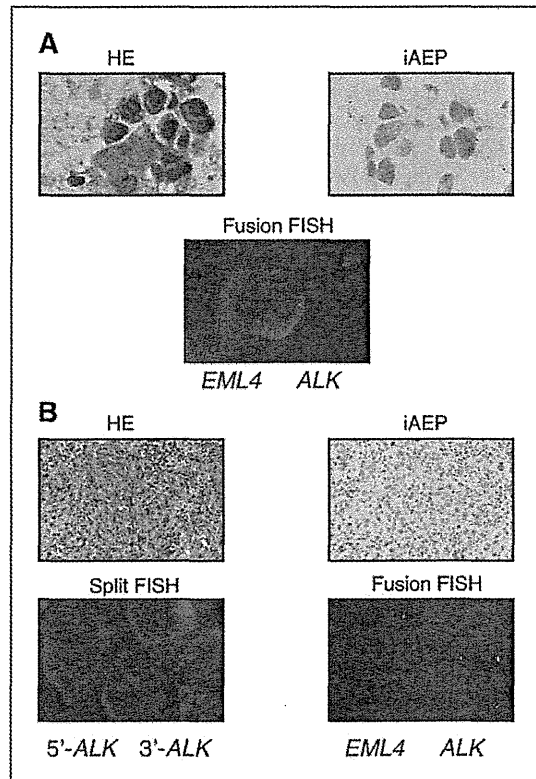

Figure 3. Specimens positive for *EML4-ALK* by RT-PCR but negative by iAEP-based IHC and by FISH. Sections of tumor biopsy specimens for J-#393 tumor (A) and J-#927 (B) were stained with hematoxylin-eosin (HE), subjected to immunohistochemical analysis by the iAEP method, and examined by split or fusion FISH. The color of fluorescence for the probes in each hybridization is indicated below the FISH images. Nuclei are stained blue with 4′,6-diamidino-2-phenylindole (DAPI).

(4.24%; Table 1, Fig. 2A). Nucleotide sequencing of each PCR product identified 19 cases positive for the E13;A20 variant, 10 cases for E6a/b;A20, a single case each for E18; A20, E20;A20, and a novel variant. *EML4-ALK* was detected in a wide range of specimens including bronchial washing fluid ($n = 11$), tumor biopsy ($n = 8$), resected tumor ($n = 7$), pleural effusion ($n = 5$), sputum ($n = 4$), and metastatic lymph node ($n = 1$). We did not detect any *KIF5B-ALK* cDNAs, confirming the rarity of this fusion gene.

Importantly, an E13;A20 product was consistently identified in both of the sputa obtained at different time points from patient J-#1. Likewise, an E13;A20 product was detected in both the tumor biopsy and sputum from patient J-#53 as well as in the pleural effusion and 2 resected tumor specimens from patient J-#330, supporting the reliability of our RT-PCR approach.

Sequence determination for the RT-PCR product from patient J-#189 revealed that exon 14 of *EML4* was fused to exon 20 of *ALK* with an intervening sequence. Genomic PCR analysis of the J-#189 specimen with a forward primer targeted to exon 14 of *EML4* and a reverse primer targeted to exon 20 of *ALK* yielded a specific product, nucleotide sequencing of which revealed that a position 453 bp downstream of *EML4* exon 14 was ligated to a position 56 bp upstream of *ALK* exon 20 (Fig. 2B). In the transcript of this

fusion gene, exon 14 of *EML4* is thus spliced to a TT sequence that is located within *EML4* intron 14 and which is directly ligated to intron 19 of *ALK*. This splicing event results in an in-frame fusion between the mRNA sequences derived from *EML4* and *ALK*. Furthermore, a full-length cDNA for this variant, here designated E14::ins2;ins56A20, was isolated by RT-PCR analysis (Supplementary Fig. S3), and the potent transforming ability of the encoded protein was confirmed with an *in vitro* focus formation assay (Supplementary Fig. S4).

Comparison between multiplex RT-PCR and sensitive IHC

Finally, we applied the iAEP method to the *EML4-ALK*–positive cases for which FFPE specimens were also available ($n = 15$). All but 2 cases (J-#393 and J-#927) manifested clear immunoreactivity with antibodies to ALK (Table 1). FISH analysis of these 2 specimens also failed to detect the *EML4-ALK* rearrangements (Fig. 3). Given that genomic DNA was not available for the tumor of patient J-#393, we

— 70 —

were not able to determine whether the PCR result was a false-positive. For J-#927, however, PCR analysis of genomic DNA with a forward primer targeted to *EML4* exon 6 and a reverse primer to *ALK* exon 20 resulted in the amplification of an approximately 8.8-kbp genomic fragment, nucleotide sequencing of which revealed a fusion event between intron 6 of *EML4* and intron 19 of *ALK* (Supplementary Fig. S5). Isolation of the genomic fusion point thus indicates that J-#927 indeed harbors an *EML4-ALK*–positive tumor.

Discussion

We have conducted a large-scale, prospective screening for *EML4-ALK* with an RT-PCR–based approach. Whereas RNA extraction and cDNA synthesis add extra labor to the diagnostic procedure, certain introns of *EML4* are too large (intron 6 spans >16 kbp, for instance) for reliable amplification by genomic PCR. We therefore adopted RT-PCR as the method for our prospective screening. Specific PCR products were successfully isolated from different types of specimen, even from sputum (J-#1, J-#53, J-#215) and washing fluid of a tumor biopsy needle (J-#530). Multiple positive results obtained with different specimens of the same individuals further reinforce the reliability of our multiplex RT-PCR system as a diagnostic tool for *EML4-ALK*–positive tumors. Importantly, a subset of *EML4-ALK*–positive individuals diagnosed in the present study entered a clinical trial for crizotinib, and the response rate of the evaluable patients ($n = 9$) was 100% with this drug, again verifying the accuracy of our RT-PCR–based diagnosis.

The frequency of *EML4-ALK* in our cohort was 4.24% for all NSCLC cases and 6.11% for lung adenocarcinoma, values similar to those obtained in previous studies (20, 21). However, our prevalence data might be overestimates because the knowledge of mutual exclusiveness for *EML4-ALK* and *EGFR* mutations may have affected patient selection for our specimen collection. Indeed, *EGFR* mutation frequency among our cohort (23.8%) is slightly lower than that (30.9%) determined in a previous large-scale screening in Japan (28).

The clinicopathologic features of patients with *EML4-ALK*–positive tumors determined in the present study are also in agreement with those previously described, with a bias toward a young age, adenocarcinoma histology, and never or light smoking. Whereas a previous large-scale screening for *EML4-ALK* based on FISH did not detect a sex preference for the fusion gene (7), our cohort revealed a significant female preference. Such a sex difference was evident even among individuals below 40 years of age ($P = 0.03$, Fisher' exact test) and among those with an adenocarcinoma histology ($P = 0.005$, Fisher' exact test). Further large-scale studies are warranted to determine whether this uneven sex distribution of *EML4-ALK* is related to particular clinicopathologic features or ethnic groups.

Given that *EML4-ALK* and *EGFR* mutations are almost mutually exclusive and that the fusion gene is enriched in lung adenocarcinoma with an early onset, it should prove to be clinically beneficial to pay special attention to such subsets of patients. Indeed, *EML4-ALK* was detected in 27.7% of *EGFR* mutation–negative adenocarcinomas in individuals of younger than 50 years and in 50.0% of those in individuals of younger than 40 years in our cohort. Given the marked efficacy of ALK inhibitors in patients with *EML4-ALK*–positive NSCLCs (7), however, physicians should not dismiss the diagnosis in other subsets of patients. For example, *EML4-ALK* was even detected in an 80-year-old woman and in another woman with an intense smoking history (82 pack-years; Table 1).

Multiplex RT-PCR has both advantages and disadvantages compared with other techniques. Importantly, the accuracy of RT-PCR–based diagnosis depends markedly on the RNA quality of specimens. In our cohort, for instance, 71 (7.75%) of the initial 916 specimens were excluded from *EML4-ALK* screening because of a failure to obtain PCR products for RNase P (the other 37 samples were excluded because they were not NSCLCs). Low RNA quality thus clearly hampers reliable RT-PCR–based diagnosis.

Also, as expected, there was a large variation in the PCR cycle number required for successful amplification among specimens. In our cohort, 50 cycles of PCR allowed detection of PCR products for all positive cases, but such extensive amplification may also generate nonspecific products (as shown in Fig. 2A). Further optimization of primer sequences or combinations may minimize the generation of such byproducts. Furthermore, whereas our system should be able to capture all in-frame fusions of *ALK* to *EML4* or *KIF5B*, it is not capable in its present form of detecting *ALK* fusions to other partners, such as *KLC1-ALK*, which was recently shown to be present infrequently in NSCLCs (29).

On the other hand, RT-PCR can be readily applied to specimens such as sputum, bronchial washing fluid, or pleural effusion that may not be suitable for preparation of FFPE samples. Whereas the latter 2 specimen types can be used for the preparation of cell blocks suitable for analysis by FISH or IHC, this procedure may not be as widely adopted in the clinic as is FISH or IHC. More importantly, it is difficult to generate cell blocks or FFPE samples from sputum. Our current prospective screening identified 4 *EML4-ALK*–positive sputa of 35 samples (Table 1, Supplementary Fig. S1), showing that sputum is a suitable specimen for RT-PCR analysis. Indeed, sputum was the only available specimen from patient J-#215 both for the diagnosis of NSCLCs and for the detection of *EML4-ALK*. If RT-PCR had not been applied to this patient's sputum, we would not have been able to identify her tumor as positive for *EML4-ALK*, and she would not have had the chance to receive treatment with an ALK inhibitor in Japan.

Furthermore, PCR-based detection of *EML4-ALK* should have a higher analytic sensitivity compared with IHC or FISH (Fig. 1B). Even with sputum obtained from a patient with chronic bronchitis, RT-PCR was able to readily detect *EML4-ALK* at a concentration of 10 positive cells/mL (1). Thus, provided that RNA is not substantially degraded, RT-PCR–based diagnosis is expected to have a strong advantage

with regard to the detection of low numbers of *EML4-ALK*-positive cells.

Ideally, every NSCLC case should be examined for the presence of *EML4-ALK*, with a sensitive and accurate diagnostic strategy for the oncogenic fusion being essential for the adoption of ALK inhibitors in the clinic. Given the reliable detection of *EML4-ALK* mRNA by multiplex RT-PCR shown in the present study, we propose the following scheme for the comprehensive diagnosis of *EML4-ALK*-positive NSCLCs. For sputum, bronchial lavage fluid, pleural effusion, or other specimens that may not be suitable for the preparation of FFPE tissue, multiplex RT-PCR should be applied to detect *ALK* fusion mRNAs. In contrast, given that FFPE specimens usually have fragmented RNA, they should be subjected to FISH and to sensitive immunohistochemical analysis such as that described previously (14, 15). Furthermore, FISH or IHC can be applied to cell blocks prepared from some non-FFPE specimens. No single technique is therefore able to detect *EML4-ALK* in all types of specimen, and appropriate tests should be chosen on the basis of the specimens available for a given patient.

Disclosure of Potential Conflicts of Interest

H. Mano is the CEO of CureGene Co., Ltd.; has commercial research grant from Illumina, Inc. and Astellas Pharma Inc.; has ownership interest (including patents); and is on the consultant/advisory board of Chugai Pharma-

References

1. Soda M, Choi YL, Enomoto M, Takada S, Yamashita Y, Ishikawa S, et al. Identification of the transforming *EML4-ALK* fusion gene in non-small-cell lung cancer. Nature 2007;448:561–6.
2. Mano H. ALKoma: a cancer subtype with a shared target. Cancer Discov 2012;2:495–502.
3. Shaw AT, Solomon B. Targeting anaplastic lymphoma kinase in lung cancer. Clin Cancer Res 2011;17:2081–6.
4. Soda M, Takada S, Takeuchi K, Choi YL, Enomoto M, Ueno T, et al. A mouse model for *EML4-ALK*-positive lung cancer. Proc Natl Acad Sci U S A 2008;105:19893–7.
5. Chen Z, Sasaki T, Tan X, Carretero J, Shimamura T, Li D, et al. Inhibition of ALK, PI3K/MEK, and HSP90 in murine lung adenocarcinoma induced by EML4-ALK fusion oncogene. Cancer Res 2010;70:9827–36.
6. Marzec M, Kasprzycka M, Ptasznik A, Wlodarski P, Zhang Q, Odum N, et al. Inhibition of ALK enzymatic activity in T-cell lymphoma cells induces apoptosis and suppresses proliferation and STAT3 phosphorylation independently of Jak3. Lab Invest 2005;85:1544–54.
7. Kwak EL, Bang YJ, Camidge DR, Shaw AT, Solomon B, Maki RG, et al. Anaplastic lymphoma kinase inhibition in non-small-cell lung cancer. N Engl J Med 2010;363:1693–703.
8. Katayama R, Khan TM, Benes C, Lifshits E, Ebi H, Rivera VM, et al. Therapeutic strategies to overcome crizotinib resistance in non-small cell lung cancers harboring the fusion oncogene EML4-ALK. Proc Natl Acad Sci U S A 2011;108:7535–40.
9. Lovly CM, Heuckmann JM, de Stanchina E, Chen H, Thomas RK, Liang C, et al. Insights into ALK-driven cancers revealed through development of novel ALK tyrosine kinase inhibitors. Cancer Res 2011;71:4920–31.
10. Sakamoto H, Tsukaguchi T, Hiroshima S, Kodama T, Kobayashi T, Fukami TA, et al. CH5424802, a selective ALK inhibitor capable of blocking the resistant gatekeeper mutant. Cancer Cell 2011;19:679–90.
11. Gerber DE, Minna JD. ALK inhibition for non-small cell lung cancer: from discovery to therapy in record time. Cancer Cell 2010;18:548–51.

12. Butrynski JE, D'Adamo DR, Hornick JL, Dal Cin P, Antonescu CR, Jhanwar SC, et al. Crizotinib in ALK-rearranged inflammatory myofibroblastic tumor. N Engl J Med 2010;363:1727–33.
13. Mok TS, Wu YL, Thongprasert S, Yang CH, Chu DT, Saijo N, et al. Gefitinib or carboplatin-paclitaxel in pulmonary adenocarcinoma. N Engl J Med 2009;361:947–57.
14. Takeuchi K, Choi YL, Togashi Y, Soda M, Hatano S, Inamura K, et al. KIF5B-ALK, a novel fusion oncokinase identified by an immunohistochemistry-based diagnostic system for ALK-positive lung cancer. Clin Cancer Res 2009;15:3143–9.
15. Mino-Kenudson M, Chirieac LR, Law K, Hornick JL, Lindeman N, Mark EJ, et al. A novel, highly sensitive antibody allows for the routine detection of ALK-rearranged lung adenocarcinomas by standard immunohistochemistry. Clin Cancer Res 2010;16:1561–71.
16. Nagai Y, Miyazawa H, Huqun, Tanaka T, Udagawa K, Kato M, et al. Genetic heterogeneity of the epidermal growth factor receptor in non-small cell lung cancer cell lines revealed by a rapid and sensitive detection system, the peptide nucleic acid-locked nucleic acid PCR clamp. Cancer Res 2005;65:7276–82.
17. Shaw AT, Yeap BY, Mino-Kenudson M, Digumarthy SR, Costa DB, Heist RS, et al. Clinical features and outcome of patients with non-small-cell lung cancer who harbor EML4-ALK. J Clin Oncol 2009;27:4247–53.
18. Horn L, Pao W. EML4-ALK: honing in on a new target in non-small-cell lung cancer. J Clin Oncol 2009;27:4232–5.
19. Tiseo M, Gelsomino F, Boggiani D, Bortesi B, Bartolotti M, Bozzetti C, et al. EGFR and EML4-ALK gene mutations in NSCLC: a case report of erlotinib-resistant patient with both concomitant mutations. Lung Cancer (Amsterdam, the Netherlands) 2011;71:241–3.
20. Inamura K, Takeuchi K, Togashi Y, Hatano S, Ninomiya H, Motoi N, et al. EML4-ALK lung cancers are characterized by rare other mutations, a TTF-1 cell lineage, an acinar histology, and young onset. Mod Pathol 2009;22:508–15.
21. Wong DW, Leung EL, So KK, Tam IY, Sihoe AD, Cheng LC, et al. The EML4-ALK fusion gene is involved in various histologic types of lung

— 73 —

cancers from nonsmokers with wild-type EGFR and KRAS. Cancer 2009;115:1723–33.

22. Choi YL, Takeuchi K, Soda M, Inamura K, Togashi Y, Hatano S, et al. Identification of novel isoforms of the *EML4-ALK* transforming gene in non-small cell lung cancer. Cancer Res 2008;68:4971–6.

23. Koivunen JP, Mermel C, Zejnullahu K, Murphy C, Lifshits E, Holmes AJ, et al. EML4-ALK fusion gene and efficacy of an ALK kinase inhibitor in lung cancer. Clin Cancer Res 2008;14:4275–83.

24. Takeuchi K, Choi YL, Soda M, Inamura K, Togashi Y, Hatano S, et al. Multiplex reverse transcription-PCR screening for *EML4-ALK* fusion transcripts. Clin Cancer Res 2008;14:6618–24.

25. Lin E, Li L, Guan Y, Soriano R, Rivers CS, Mohan S, et al. Exon array profiling detects EML4-ALK fusion in breast, colorectal, and non-small cell lung cancers. Mol Cancer Res 2009;7:1466–76.

26. Takahashi T, Sonobe M, Kobayashi M, Yoshizawa A, Menju T, Nakayama E, et al. Clinicopathologic features of non-small-cell lung cancer with EML4-ALK fusion gene. Ann Surg Oncol 2010;17:889–97.

27. Sanders HR, Li HR, Bruey JM, Scheerle JA, Meloni-Ehrig AM, Kelly JC, et al. Exon scanning by reverse transcriptase-polymerase chain reaction for detection of known and novel EML4-ALK fusion variants in non-small cell lung cancer. Cancer Genet 2011;204:45–52.

28. Toyooka S, Matsuo K, Shigematsu H, Kosaka T, Tokumo M, Yatabe Y, et al. The impact of sex and smoking status on the mutational spectrum of epidermal growth factor receptor gene in non small cell lung cancer. Clin Cancer Res 2007;13:5763–8.

29. Togashi Y, Soda M, Sakata S, Sugawara E, Hatano S, Asaka R, et al. KLC1-ALK: a novel fusion in lung cancer identified using a formalin-fixed paraffin-embedded tissue only. PLoS One 2012;7:e31323.

nature
medicine

A common *BIM* deletion polymorphism mediates intrinsic resistance and inferior responses to tyrosine kinase inhibitors in cancer

King Pan Ng[1,23], Axel M Hillmer[2,23], Charles T H Chuah[1,3,23], Wen Chun Juan[1,23], Tun Kiat Ko[1], Audrey S M Teo[2], Pramila N Ariyaratne[2], Naoto Takahashi[4], Kenichi Sawada[4], Yao Fei[2,5], Sheila Soh[1], Wah Heng Lee[2], John W J Huang[1], John C Allen Jr[6], Xing Yi Woo[2], Niranjan Nagarajan[2], Vikrant Kumar[2], Anbupalam Thalamuthu[2], Wan Ting Poh[2], Ai Leen Ang[3], Hae Tha Mya[3], Gee Fung How[3], Li Yi Yang[3], Liang Piu Koh[7], Balram Chowbay[8], Chia-Tien Chang[1], Veera S Nadarajan[9], Wee Joo Chng[7,10,11], Hein Than[3], Lay Cheng Lim[3], Yeow Tee Goh[3], Shenli Zhang[1], Dianne Poh[1], Patrick Tan[1,2,11], Ju-Ee Seet[12], Mei-Kim Ang[13], Noan-Minh Chau[13], Quan-Sing Ng[13], Daniel S W Tan[13], Manabu Soda[14], Kazutoshi Isobe[15], Markus M Nöthen[16], Tien Y Wong[17], Atif Shahab[2], Xiaoan Ruan[2], Valère Cacheux-Rataboul[2], Wing-Kin Sung[2], Eng Huat Tan[13], Yasushi Yatabe[18], Hiroyuki Mano[14,19], Ross A Soo[7,11], Tan Min Chin[7], Wan-Teck Lim[13,20], Yijun Ruan[2,21] & S Tiong Ong[1,3,13,22]

Tyrosine kinase inhibitors (TKIs) elicit high response rates among individuals with kinase-driven malignancies, including chronic myeloid leukemia (CML) and epidermal growth factor receptor–mutated non–small-cell lung cancer (EGFR NSCLC). However, the extent and duration of these responses are heterogeneous, suggesting the existence of genetic modifiers affecting an individual's response to TKIs. Using paired-end DNA sequencing, we discovered a common intronic deletion polymorphism in the gene encoding BCL2-like 11 (BIM). BIM is a pro-apoptotic member of the B-cell CLL/lymphoma 2 (BCL2) family of proteins, and its upregulation is required for TKIs to induce apoptosis in kinase-driven cancers. The polymorphism switched *BIM* splicing from exon 4 to exon 3, which resulted in expression of *BIM* isoforms lacking the pro-apoptotic BCL2-homology domain 3 (BH3). The polymorphism was sufficient to confer intrinsic TKI resistance in CML and EGFR NSCLC cell lines, but this resistance could be overcome with BH3-mimetic drugs. Notably, individuals with CML and EGFR NSCLC harboring the polymorphism experienced significantly inferior responses to TKIs than did individuals without the polymorphism ($P = 0.02$ for CML and $P = 0.027$ for EGFR NSCLC). Our results offer an explanation for the heterogeneity of TKI responses across individuals and suggest the possibility of personalizing therapy with BH3 mimetics to overcome *BIM*-polymorphism–associated TKI resistance.

The use of TKIs has elicited remarkable therapeutic responses in individuals presenting with a broad range of malignancies driven by oncogenic kinases[1]. However, before the use of TKIs, such malignancies were regarded as highly chemoresistant, as exemplified by breakpoint cluster region (BCR)–c-abl oncogene 1, non-receptor tyrosine kinase (ABL1) kinase-driven CML and EGFR NSCLC[2,3]. After the advent of TKIs, treatment responses in both of these cancers typically approached 80% (refs. 4,5). These clinical observations emphasized the importance of classifying tumors according to their molecular drivers and at the same time stimulated the search for biomarkers that could identify the 20% of individuals at risk for primary or intrinsic TKI resistance, as well as guide therapy to overcome this resistance.

[1]Cancer & Stem Cell Biology Signature Research Programme, Duke–National University of Singapore (NUS) Graduate Medical School, Singapore. [2]Genome Institute of Singapore, Singapore. [3]Department of Haematology, Singapore General Hospital, Singapore. [4]Department of Hematology, Nephrology and Rheumatology, Akita University Graduate School of Medicine, Akita, Japan. [5]Department of Epidemiology and Public Health, Yong Loo Lin School of Medicine, National University of Singapore, Singapore. [6]Centre for Quantitative Medicine, Duke-NUS Graduate Medical School, Singapore. [7]Department of Hematology-Oncology, National University Cancer Institute of Singapore, National University Health System, Singapore. [8]Clinical Pharmacology Laboratory, National Cancer Centre, Singapore. [9]University of Malaya, Kuala Lumpur, Malaysia. [10]Department of Medicine, Yong Loo Lin School of Medicine, National University of Singapore, Singapore. [11]Cancer Science Institute of Singapore, National University of Singapore, Singapore. [12]Department of Pathology, National University Health System, Singapore. [13]Department of Medical Oncology, National Cancer Centre, Singapore. [14]Division of Functional Genomics, Jichi Medical University, Tochigi, Japan. [15]Department of Respiratory Medicine, Toho University Omori Medical Center, Tokyo, Japan. [16]Institute of Human Genetics, University of Bonn, Bonn, Germany. [17]Singapore Eye Research Institute, Singapore National Eye Centre and National University Health System, Singapore. [18]Department of Pathology and Molecular Diagnostics, Aichi Cancer Center, Aichi, Japan. [19]Department of Medical Genomics, Graduate School of Medicine, University of Tokyo, Tokyo, Japan. [20]Office of Clinical Sciences, Duke-NUS Graduate Medical School, Singapore. [21]Department of Biochemistry, National University of Singapore, Singapore. [22]Department of Medicine, Division of Medical Oncology, Duke University Medical Center, Durham, North Carolina, USA. [23]These authors contributed equally to this work. Correspondence should be addressed to Y.R. (ruanj@gis.a-star.edu.sg), W.-T.L. (dmolwt@nccs.com.sg) or S.T.O. (sintiong.ong@duke-nus.edu.sg).

– 74 –

ARTICLES

In this respect, we note that although polymorphisms in genes regulating drug metabolism provide useful information to modify the dosing of therapeutic agents[6], few examples exist in the germline that predict response to targeted therapies.

Accordingly, we investigated whether polymorphisms affecting TKI sensitivity might account for the 20% of TKI-treated individuals with poor responses and whether these polymorphisms might be enriched among genes that are crucial in the apoptotic response to TKIs. One such candidate gene is *BCL2L11* (also known as *BIM*), which encodes a BH3-only protein that is a BCL2 family member. The BH3-only proteins activate cell death by either opposing the prosurvival members of the BCL2 family (BCL2, BCL2-like 1 (BCL-XL, also known as BCL2L1), myeloid cell leukemia sequence 1 (MCL1) and BCL2-related protein A1 (BCL2A1)) or by binding to the pro-apoptotic BCL2 family members (BCL2-associated X protein (BAX) and BCL2-antagonist/killer 1 (BAK1)) and directly activating their pro-apoptotic functions[7]. Others have previously shown that several kinase-driven cancers, including CML and EGFR NSCLC, maintain a survival advantage by suppressing *BIM* transcription and by targeting BIM protein for proteasomal degradation through mitogen-activated protein kinase 1 (MAPK1)-dependent phosphorylation[8–13]. Furthermore, in all of these malignancies, BIM upregulation is required for TKIs to induce apoptosis, and suppression of BIM expression is sufficient to confer *in vitro* TKI resistance[8–13].

Here we describe the discovery of a common deletion polymorphism in the *BIM* gene that results in the generation of alternatively spliced isoforms of BIM that lack the crucial BH3 domain. This polymorphism has a profound effect on the TKI sensitivity of CML and EGFR NSCLC cells, such that one copy of the deleted allele is sufficient to render cells intrinsically TKI resistant. We show that individuals with the polymorphism have markedly inferior responses to TKI than do individuals without the polymorphism. Specifically, the polymorphism correlated with a lesser degree of response to imatinib, a TKI, in CML as well as a shorter progression-free survival (PFS) with EGFR TKI therapy in EGFR NSCLC.

RESULTS

A new *BIM* deletion polymorphism in resistant CML samples

To identify new TKI-resistance mechanisms in CML, we used massively parallel DNA sequencing of paired-end ditags[14,15] to interrogate
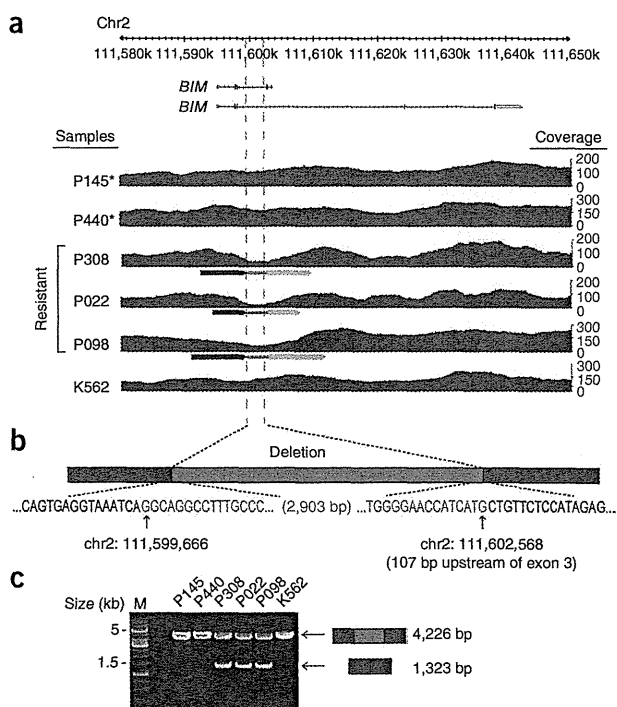
the genomes of five CML samples obtained from subjects who were either sensitive to or resistant to treatment with TKIs (**Supplementary Tables 1 and 2**). We identified the BCR-ABL1 translocation in all CML samples, but not in control samples from patients in complete remission, and we also identified several CML-specific structural variations (**Supplementary Fig. 1** and **Supplementary Tables 3–6**).

Among the structural variations that were common to all the TKI-resistant samples, one in particular attracted our attention because it occurred in intron 2 of the *BIM* gene (**Fig. 1a**). This structural variation comprised an identical 2,903-bp genomic deletion that was common to all three resistant samples (**Fig. 1a–c**), suggesting that it was germline and polymorphic. After screening 2,597 healthy individuals, we found the deletion polymorphism to occur commonly in East Asian individuals (12.3% carrier frequency), but it was absent in individuals from African and European populations (0%) (**Supplementary Table 7**).

Functional effects of the *BIM* deletion polymorphism

Inspection of *BIM* gene structure suggested that the splicing of exon 3 and the splicing of exon 4 occur in a mutually exclusive manner because of the presence of a stop codon and a polyadenylation signal within exon 3 (**Fig. 2a** and **Supplementary Fig. 2a**)[16,17]. Indeed, sequencing of all identifiable *BIM* transcripts in CML cells confirmed that exons 3 and 4 never occurred in the same transcript (**Supplementary Fig. 2b**), consistent with prior reports[17]. Because of its close proximity (107 bp) to the intron-exon boundary at the 5′ end of exon 3, we hypothesized that the deletion polymorphism would result in preferential splicing of exon 3 over exon 4 (**Fig. 2a**)[18]. To determine whether this was the case, we constructed a minigene to assess whether the deletion leads to the preferential inclusion of exon 3 over exon 4 (**Fig. 2b**)[19] and found that the presence of the deletion favored splicing to exon 3 over exon 4 by at least fivefold (**Fig. 2c**). Notably, primary cells from individuals with CML showed the same phenomenon, as evidenced by the fact that polymorphism-containing

Figure 1 A 2,903-bp deletion polymorphism in intron 2 of *BIM* is present in TKI-resistant CML samples. (a) A Genome Browser view of the DNA–paired-end tag (PET) data encompassing chromosome 2 111,580,000–111,650,000 bp from the five clinical CML samples and K562 cells. Detection of the *BIM* deletion polymorphism by DNA-PET analysis in three of three samples from individuals with resistance to imatinib (P308, P022 and P098) but not in samples from subjects or cell lines that are sensitive to imatinib (P145, P440 and K562). The asterisks indicate that the samples (P145 and P440) were obtained from the same individual at presentation in chronic phase CML and when in major molecular remission, respectively. The red tracks represent the number of the sequenced concordant PETs that map to the region (coverage). The burgundy and pink horizontal arrowheads connected by green lines represent mapping regions of discordant PETs and indicate the presence of a deletion. The vertical dashed lines depict the deleted region. (b) Schematic depicting the intronic *BIM* deletion polymorphism and its flanking sequences. The breakpoints were identified by Sanger sequencing of PCR products. Deleted sequences are highlighted in blue. The human reference sequence coordinates are based on NCBI Build 36. (c) Agarose gel showing the PCR products from the five subject samples and K562 cells using primers that flanked the deletion. PCR products with a size of 4,226 bp and 1,323 bp correspond to the alleles without and with the deletion, respectively. The presence of both the 4,226-bp and 1,323-bp products indicates that the individual is heterozygous for the deletion polymorphism.

a Chr2

111,580k 111,590k 111,600k 111,610k 111,620k 111,630k 111,640k 111,650k

BIM
BIM

Samples — Coverage

Resistant
P145*
P440*
P308
P022
P098
K562

b
Deletion

...CAGTGAGGTAAATCAGGCAGGCCTTTGCCC... (2,903 bp) ...TGGGGAACCATCATGCTGTTCTCCATAGAG...

chr2: 111,599,666   chr2: 111,602,568 (107 bp upstream of exon 3)

c
Size (kb) M   P145 P440 P308 P022 P098 K562

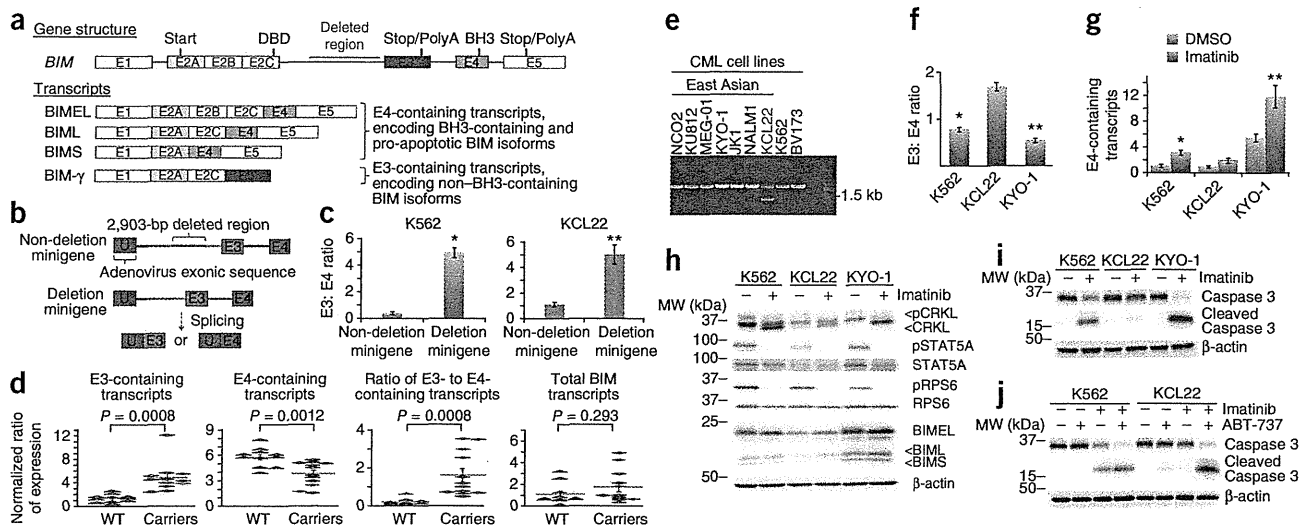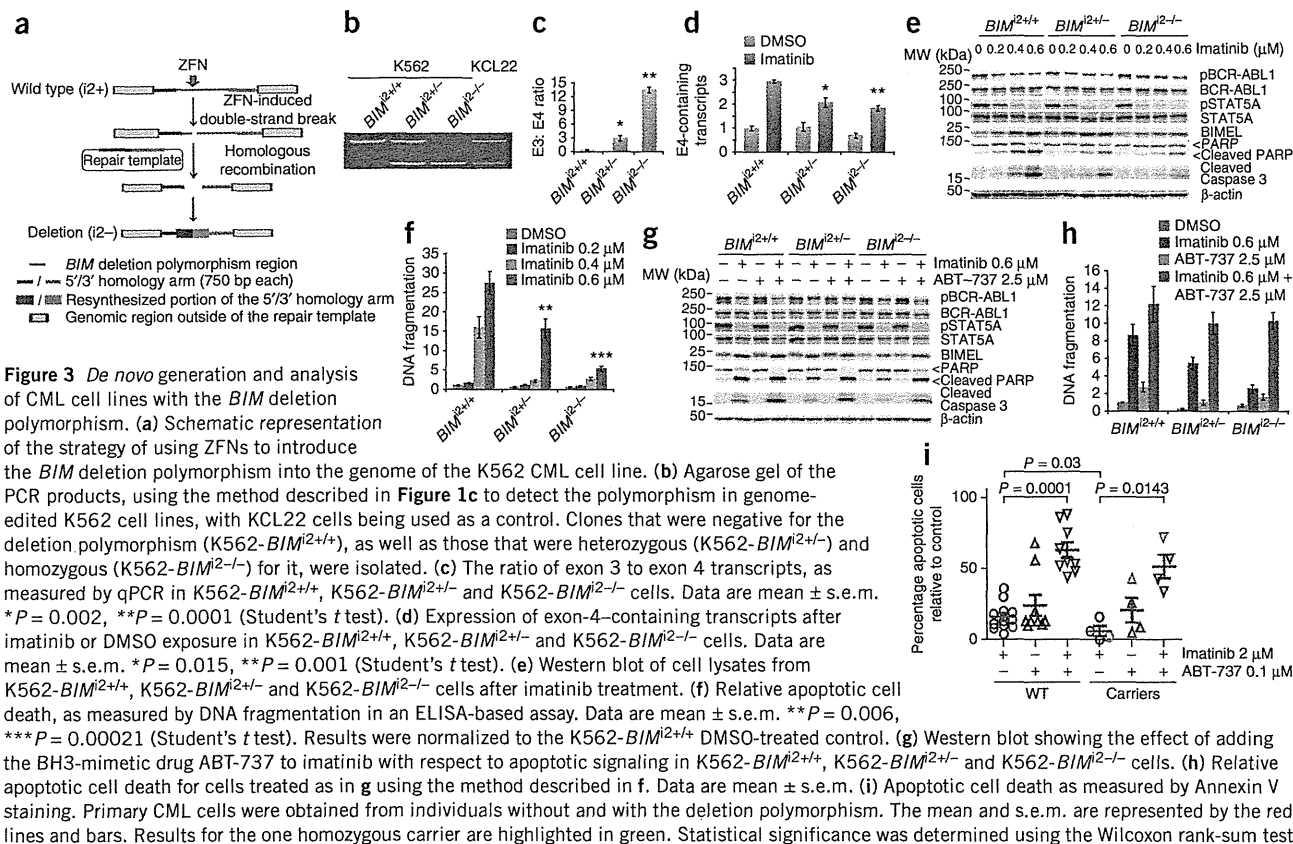5 -   ← 4,226 bp
1.5 -   ← 1,323 bp

— 75 —

Figure 2 Effects of the deletion polymorphism on *BIM* gene function. (a) Genomic organization of *BIM* (top) showing exons for the major *BIM* transcript splice isoforms (bottom), including BIMEL, BIML and BIMS, as well as BIM-γ, which lacks the BH3 domain[17]. The deletion polymorphism between exons 2 and 3 is highlighted with a red line. The exons containing the start codon (start), the dynein-binding domain (DBD), the BH3 domain (BH3) and the stop codon and polyadenylation signal sequences (Stop/PolyA) are also highlighted. Exon 4 encodes for the BH3 domain that is required for BIM apoptotic function, whereas exon 3 lacks this domain. Because exon 3 and exon 4 undergo mutually exclusive splicing, exon-3–containing transcripts will not contain a BH3 domain. The diagram is not drawn to scale. E, exon. (b) Schematic of the two minigene constructs used for measuring splicing to exons 3 and 4. (c) The increased ratio of exon 3 to exon 4 transcripts in the non-deletion minigene construct compared to the deletion minigene construct in K562 cells (left) and in KCL22 cells (right). Data are mean ± s.e.m. $*P = 0.0002$, $**P = 0.012$ (Student's *t* test). (d) Expression of exon-specific transcripts of *BIM* in 23 samples from subjects with CML. $n = 11$ subjects without the deletion (WT), and $n = 12$ subjects with the deletion (carriers). The amounts of the various transcripts containing exons 2A, 3 or 4 are expressed as normalized ratios relative to exon 2A (for exons 3 and 4) or β-actin (ACTB, for exon 2A (total *BIM* transcripts). We measured exon 2A transcripts as a readout for all *BIM* transcripts, as exon 2A contains the start site and is present in all transcripts. The mean and s.e.m. are represented by the red lines and bars. The expressions for the one homozygous carrier are highlighted in green. Statistical significance was determined using the Wilcoxon rank-sum test. (e) Agarose gel of the PCR products, using the method described in **Figure 1c**, to detect the polymorphism in a collection of East Asian and non–East Asian CML cell lines. The KCL22 line carries the deletion polymorphism and is highlighted in red. (f) Ratio of exon-3– to exon-4–containing transcripts in CML cell lines with (KCL22) and without (K562 and KYO-1) the deletion polymorphism. Data are mean ± s.e.m. $*P = 0.016$, $**P = 0.011$ (Student's *t* test). (g) The expression of exon-4–specific transcripts of *BIM* (normalized to β-actin), as measured by quantitative PCR (qPCR) in cell lines with and without the deletion polymorphism treated with DMSO or imatinib. Data are mean ± s.e.m. $*P = 0.01$, $**P = 0.004$ (Student's *t* test) with respect to imatinib-treated KCL22 cells. (h) Western blot showing upregulation of BIM and the inhibition of signaling pathways downstream of BCR-ABL1 kinase in CML cell lines as a result of imatinib treatment. CRKL, v-crk sarcoma virus CT10 oncogene homolog (avian)-like; pCRKL, phosphorylated CRKL; STAT5A, signal transducer and activator of transcription 5A; pSTAT5A, phosphorylated STAT5A; RPS6, ribosomal protein S6; pRPS6, phosphorylated RPS6; MW, molecular weight. (i) Western blot showing caspase 3 cleavage in cells treated as in **h**. (j) Western blot showing caspase 3 cleavage in cell lines treated with imatinib and with or without the BH3-mimetic drug ABT-737.

samples had higher expression of exon-3– compared to exon-4–containing transcripts, whereas general *BIM* transcription was unaffected by the polymorphism (**Fig. 2d**). We observed similar results in lymphoblastoid cell lines obtained from normal healthy HapMap individuals, indicating that the polymorphism has a cell-lineage–independent effect (**Supplementary Fig. 2c**). Taken together, these results suggest that the 2.9-kb deleted region contains *cis* elements that suppress the splicing of *BIM* exon 3, which, in cells harboring the deletion, results in preferential splicing of exon 3 over exon 4.

Because the pro-apoptotic BH3 domain is encoded exclusively by exon 4 of *BIM* (**Fig. 2a**)[17] and is required for BIM's apoptotic function[20,21], our observations suggest a previously unidentified mechanism for TKI resistance. In this model, after TKI exposure, polymorphism-containing CML cells would favor the expression of exon-3– over exon-4–containing *BIM* transcripts, resulting in decreased expression of BH3-containing BIM isoforms and, consequently, impaired BH3-domain–dependent apoptosis. To facilitate the study of this issue, we identified a Japanese CML cell line, KCL22 (ref. 22), that contained the deletion (**Fig. 2e**) and confirmed that cells from the line expressed an increased ratio of exon 3 to exon 4 transcripts compared to cells without

the deletion (**Fig. 2f**). KCL22 cells also showed a decreased induction of exon-4–containing transcripts after TKI exposure (**Fig. 2g**), as well as decreased concentrations of BIMEL protein, a major BH3-containing BIM isoform (**Fig. 2h**)[17]. Consistent with previous reports[22–24], KCL22 cells were resistant to imatinib-induced apoptosis (**Supplementary Fig. 2d**) and showed impaired apoptotic signaling after imatinib exposure despite effective BCR-ABL1 inhibition, as confirmed by a decrease in BCR-ABL1–dependent signaling (**Fig. 2h,i**)[25,26]. KCL22 cells were also exquisitely sensitive to induction of apoptosis after increased expression of exon-4–containing and, therefore, BH3-encoding (but not exon-3–containing) *BIM* isoforms (**Supplementary Fig. 2e**). This observation suggested that the impaired imatinib-induced apoptosis in KCL22 cells could be restored by the addition of BH3-mimetic drugs, which functionally mimic BH3-only proteins by binding and inhibiting pro-survival BCL2 family members[27]. As shown in **Figure 2j**, we found that this was indeed the case. In addition, we confirmed that siRNA-mediated knockdown of exon-3–containing transcripts did not sensitize KCL22 cells to imatinib, indicating that exon-3–containing isoforms probably do not have a role in TKI resistance (**Supplementary Fig. 2f–h**).

Figure 3 De novo generation and analysis of CML cell lines with the *BIM* deletion polymorphism. (a) Schematic representation of the strategy of using ZFNs to introduce the *BIM* deletion polymorphism into the genome of the K562 CML cell line. (b) Agarose gel of the PCR products, using the method described in **Figure 1c** to detect the polymorphism in genome-edited K562 cell lines, with KCL22 cells being used as a control. Clones that were negative for the deletion polymorphism (K562-*BIM*$^{i2+/+}$), as well as those that were heterozygous (K562-*BIM*$^{i2+/-}$) and homozygous (K562-*BIM*$^{i2-/-}$) for it, were isolated. (c) The ratio of exon 3 to exon 4 transcripts, as measured by qPCR in K562-*BIM*$^{i2+/+}$, K562-*BIM*$^{i2+/-}$ and K562-*BIM*$^{i2-/-}$ cells. Data are mean ± s.e.m. *$P = 0.002$, **$P = 0.0001$ (Student's t test). (d) Expression of exon-4–containing transcripts after imatinib or DMSO exposure in K562-*BIM*$^{i2+/+}$, K562-*BIM*$^{i2+/-}$ and K562-*BIM*$^{i2-/-}$ cells. Data are mean ± s.e.m. *$P = 0.015$, **$P = 0.001$ (Student's t test). (e) Western blot of cell lysates from K562-*BIM*$^{i2+/+}$, K562-*BIM*$^{i2+/-}$ and K562-*BIM*$^{i2-/-}$ cells after imatinib treatment. (f) Relative apoptotic cell death, as measured by DNA fragmentation in an ELISA-based assay. Data are mean ± s.e.m. **$P = 0.006$, ***$P = 0.00021$ (Student's t test). Results were normalized to the K562-*BIM*$^{i2+/+}$ DMSO-treated control. (g) Western blot showing the effect of adding the BH3-mimetic drug ABT-737 to imatinib with respect to apoptotic signaling in K562-*BIM*$^{i2+/+}$, K562-*BIM*$^{i2+/-}$ and K562-*BIM*$^{i2-/-}$ cells. (h) Relative apoptotic cell death for cells treated as in g using the method described in f. Data are mean ± s.e.m. (i) Apoptotic cell death as measured by Annexin V staining. Primary CML cells were obtained from individuals without and with the deletion polymorphism. The mean and s.e.m. are represented by the red lines and bars. Results for the one homozygous carrier are highlighted in green. Statistical significance was determined using the Wilcoxon rank-sum test.

The *BIM* deletion and intrinsic TKI resistance in CML cells

We next used gene targeting facilitated by zinc finger nuclease (ZFN) to precisely recreate the deletion polymorphism in the *BIM* gene of imatinib-sensitive K562 CML cells (**Fig. 3a**). We then analyzed these cells for changes in *BIM* splicing and expression, as well as for TKI-induced apoptosis. We generated subclones that were heterozygous (K562-*BIM*$^{i2+/-}$) or homozygous (K562-*BIM*$^{i2-/-}$) for the deletion polymorphism (**Fig. 3b**). We confirmed an increased ratio of exon 3 to exon 4 transcripts (**Fig. 3c**), as well as a small but reproducible increase in BIM-γ protein expression (**Supplementary Fig. 3a**), in cells from both subclones in a polymorphism-dosage–dependent manner. We attribute the low expression of BIM-γ protein, even in the cells homozygous for the deletion polymorphism, to the relatively short half-life of BIM-γ (<1 h) (**Supplementary Fig. 3b**). Cells containing the deletion polymorphism also showed decreased induction of exon-4–containing transcripts after imatinib exposure (**Fig. 3d**), as well as impaired upregulation of BIMEL protein, diminished apoptotic signaling and decreased apoptotic cell death, as measured by DNA fragmentation in an ELISA-based assay (**Fig. 3e,f** and **Supplementary Fig. 3c**). As in KCL22 cells, the combination of the BH3 mimetic ABT-737 with imatinib enhanced the ability of the latter to activate apoptosis in polymorphism-containing cells (**Fig. 3g,h**). In parallel experiments, we re-expressed the most abundant BIM isoform, BIMEL, in polymorphism-containing cells treated with or without imatinib. Analogous to the effects seen with ABT-737 treatment, the forced expression of BIMEL enhanced the ability of imatinib to activate apoptosis in deletion-containing K562 cells (**Supplementary Fig. 3d**). We also found that primary CML cells obtained from subjects with the deletion polymorphism were less sensitive to imatinib-induced death

compared to cells from individuals without the deletion and that the relative TKI resistance of the cells with the deletion could be overcome with the addition of ABT-737 (**Fig. 3i**). Taken together, our studies establish that the *BIM* deletion polymorphism impairs the apoptotic response to imatinib by biasing splicing away from BH3-containing *BIM* isoforms and that this bias is sufficient to render CML cells intrinsically resistant to imatinib. We also show that the apoptotic response to imatinib can be restored in polymorphism-containing cells by treatment with BH3-mimetic drugs.

The *BIM* deletion as a biomarker for TKI responses in CML

Next, we performed a retrospective analysis on the influence of the deletion polymorphism on TKI responses in East Asian subjects with CML. Using a group of newly diagnosed persons with chronic phase CML from two independent East Asian (Singapore and Malaysia or Japan) cohorts ($n = 203$), we compared the clinical responses to first-line therapy with a standard dose of imatinib (400 mg per day) in individuals with and without the deletion polymorphism. We classified the clinical responses according to the European LeukemiaNet (ELN) criteria (**Supplementary Table 8**)[5] and defined resistant individuals as 'suboptimal responders' or 'failures' per ELN criteria (which includes subjects who never achieve either a complete cytogenetic response or a 3-log decrease in BCR-ABL1 transcript levels), whereas sensitive individuals corresponded to ELN-defined 'optimal responders'. In both geographic cohorts, subjects with the deletion polymorphism were more likely to have resistant disease than sensitive disease compared to controls (**Table 1**). When analyzed together, the overall odds ratio for resistant disease among subjects with the deletion polymorphism compared to those without it was 2.94 ($P = 0.02$, 95% CI 1.17–7.43).

– 77 –